LEIBNIZ-INSTITUT FÜR ATMOSPHÄREN PHYSIK IAP

Mesospheric aerosol particles: Evidence from rocket and radar techniques.

Dissertation
zur
Erlangung des akademischen Grades
doctor rerum naturalium (Dr. rer. nat.)
der Mathematisch-Naturwissenschaftlichen Fakultät
der Universität Rostock

vorgelegt von
Irina Strelnikova, geb. am 13.09.1976 in Novosibirsk
aus Kühlungsborn

Rostock, 27.02.2009

Gutachter: Prof. Dr. Markus Rapp (Universität Rostock)
Prof. Dr. Martin Friedrich (Universität Graz, Österreich)
Prof. Dr. Jörg Gumbel (Universität Stockholm, Schweden)

verteidigt am: 08.05.2009

Contents

Chapter 1

Aerosols in the mesosphere: current knowledge and problems

The upper part of the Earth's atmosphere−namely, the mesosphere/lower thermosphere (MLT) region (roughly from 50 to 120 km), is a fascinating part of the atmosphere which is strongly influenced by energy input from above and below. This region is characterized by huge seasonal variations in temperature and very low pressures.

Gravity waves propagate upward from the troposphere and deposit their energy and momentum in the mesopause region whereby they give rise to a pronounced summer-winter pole circulation driving the polar mesopause ∼80 K away from radiative equilibrium [e.g., Stroud et al., 1959; Lindzen, 1981; Lübken, 1999]. On the other hand, solar Lyman-alpha radiation may penetrate down to altitudes of ∼70 km, thereby leading to the fact that the mesopause region coincides with the lowest layer of the ionosphere, the D-region, where significant amount of free electrons and ions exists [e.g., Brekke, 1997; Hunsucker and Hargreaves, 2002; Friedrich et al., 2004].

In addition, at least 40 tonnes of interplanetary dust enter the atmosphere each day, mostly ablating in the MLT region and recondensing to subvisible nm-size smoke particles.

This work is devoted to the investigation of the heavy particles, also referred to as aerosols, which are some of the least known constituents of the MLT region. There are two types of the aerosols in the MLT, namely meteoric smoke particles (MSP) and ice particles.

MSPs are the product of meteor ablation and later recondensation to tiny smoke particles. This process takes place continuously in the MLT over the whole Earth.

The second type of the aerosols, ice particles, can form during summer at high latitudes and only in the mesopause region, where temperatures drop below the frost point of water vapor (∼150 K). The conditions for these aerosols to be created are low temperatures, sufficient amounts of water vapor, and preexisting nuclei [see Rapp and Thomas, 2006, for a recent review]. These ice particles give rise to such phenomena as noctilucent clouds (NLC) and polar mesosphere summer echoes (PMSE) [e.g., Gadsden and Schröder, 1989; Rapp and Lübken, 2004].

The observations of mesospheric ice clouds are potentially sensitive indicators of global change and solar cycle effects in the middle atmosphere [DeLand et al., 2007; Shettle et al., 2009]. Interpretation of corresponding measurements, however, critically relies on a rigorous understanding of the relevant microphysical processes where fundamental gaps in our understanding still exist. Thus, it is important to investigate the microphysical processes governing the life cycle of mesospheric ice clouds. The first step in this cycle is nucleation of ice particles which is commonly assumed to involve MSPs.

MSPs are not only potential nuclei for ice particles, it has been suggested that they provide

the surface area for heterogeneous chemistry controlling key atmospheric species such as water vapor [Summers and Siskind, 1999]. In addition, MSPs play an important role in the chemistry of the well known metal layers, where they are thought to be an efficient sink controlling the bottom height of the layers [Plane, 2004].

Despite the obvious scientific interest in meteoric smoke particles, very little is known about their properties. The main reasons for this lack of knowledge are the tiny dimensions and low densities of the MSPs making them hard to detect with optical instruments.

Thus, the main objective of this thesis is the development and application of new measurement techniques allowing to quantify the amount (number densities and sizes) of MSPs in the mesosphere.

The thesis is organized as follows.

In Section 2 the main steps playing the key role in meteoric smoke formation are reviewed: the meteor influx, meteor ablation, recondensation and growth, and transport of these particles. All these processes are connected with a number of uncertainties that create even larger uncertainties in the final estimation of the total amount of the meteoric smoke entering the Earth's atmosphere. The available measurements to date are summarized in Section 2.4. These measurements confirm the existence of charged MSPs in the mesosphere, but a quantitative comparison of them with models is still a difficult task. Also, the total number of existing measurements (eleven, including ECOMA) do not provide a sufficient statistical and geographical coverage. This underlines the necessity to conduct new measurements and to employ new techniques.

In Section 3 a review of current knowledge on the second type of the aerosols (ice particles) and their formation is presented. It was shown that in spite of significant advances during recent years, there are still many open scientific questions. One of the important questions addressed in this work regards the condensation nuclei for these ice particles. Among the many candidates that have been proposed as these nuclei, the above mentioned nanometer-size MSPs are considered the most likely.

In Section 3.1 the physics of NLC and PMSE is shortly reviewed. The standard theory of PMSE [e.g. Rapp and Lübken, 2004] requires the presence of charged ice particles. In the presented work this theory is tested and verified by a new technique for charged particle detection by means of incoherent scatter radar (ISR).

In Section 4 the main problems concerning the MLT aerosols are summarized and the detailed objectives for this thesis are defined. The thesis includes results of three sounding rocket campaigns and numerous independent incoherent scatter radar (ISR) measurements.

In the frame of this work two new techniques to measure MSPs were developed. The description of the new methods and first results from rockets (Section 5.1) and radars (Section 5.2) are summarized in Section 5 and are presented in detail in the papers collected in the Appendix.

Finally, the main findings of this work and future plans are outlined in Section 6.

Chapter 2

Meteoric smoke particles

Every day, the Earths atmosphere is hit by 10-100 tons of meteoric material. Most of it comes in the form of small meteoroid particles with sizes smaller than 1 mm. These particles come with speeds in the range of 10-70 km/s [Rosinski and Snow, 1961; Hughes, 1997; Janches et al., 2006; Mathews et al., 2008]. Collisions with air molecules heat the particles to temperatures high enough to vaporise them. This happens at heights between 70 and 100 km, in a part of the atmosphere that is known as the mesosphere [see Gabrielli et al., 2004, for a recent review]. During this evaporation process larger particles can glow so brightly that they become visible from the ground as shooting stars.

Meteoroid particles mainly consist of metals like iron, silicon, potassium, sodium and various oxides. Thus, the evaporated material forms metal layers in the upper mesosphere. These layers are well known and can be observed with ground-based instruments like lidars [Plane, 2003].

Rosinski and Snow [1961] suggested that meteoroid ablation products could recondense and form solid nanometer-scale smoke particles in the upper mesosphere. These recondensed particles are commonly called *meteoric smoke particles* (MSPs). They are assumed to follow the general motion (advection) of the air. Sooner or later this motion can transport the smoke particles down to the lower atmosphere where they can be taken up by clouds and finally rain out of the atmosphere.

A schematic picture of the interactions believed to take place once meteoric material enters the Earths atmosphere is shown in Fig. 2.1.

The MSPs have been suggested to be important for a variety of atmospheric phenomena:

- MSPs have been suggested to be the most likely candidates for the nuclei of mesospheric ice particles [see Rapp and Thomas, 2006, for a recent review].
- It has been speculated that MSPs may provide surface area on which heterogeneous chemical reactions take place and may, for example, influence the water vapor distribution in the mid-mesosphere [Summers and Siskind, 1999].
- State of the art models of mesospheric metal layers show that the observed bottom scale height of these layers can only be explained if the uptake of metals on the surface of MSPs is invoked as an effective sink of the metal atoms [Plane, 2004].
- Analysis of iridium concentrations in ice cores suggests that meteoric matter is preferentially deposited in the polar ice caps in the form of MSPs which are being transported by the mesospheric meridional circulation which, in turn, determines the latitudinal and seasonal variation of the MSP distribution [Gabrielli et al., 2004; Megner et al., 2006].

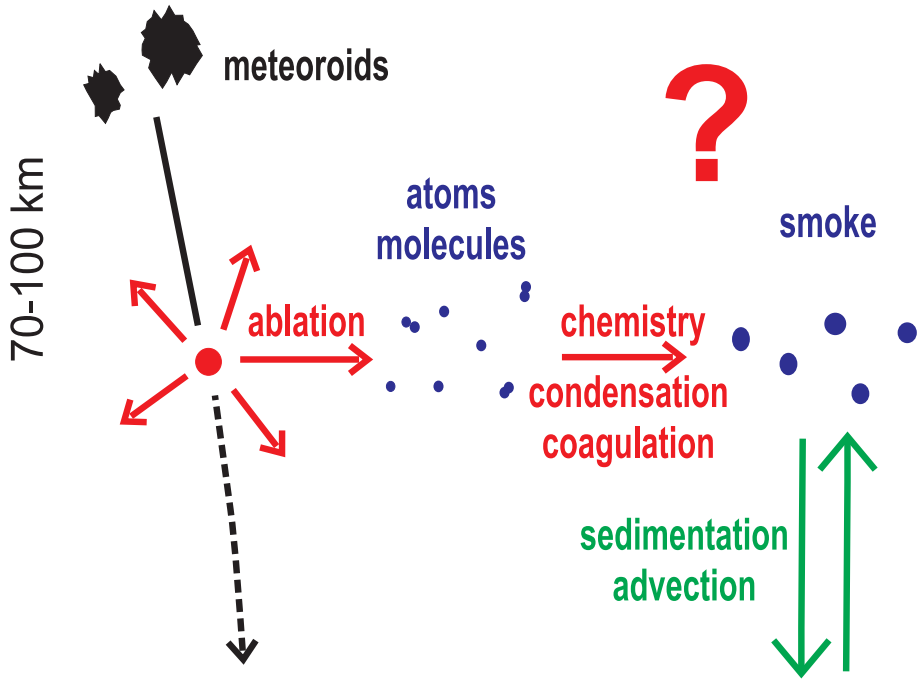

Figure 2.1: Fate of the meteoric material entering the Earth's atmosphere (taken from Megner et al. [2006]).

Recently, this idea has been further corroborated by measurements of the isothermal remanent magnetization of Greenland ice, which can only be accounted for by the presence of extraterrestrial magnetic particles in the diameter range of a few nanometers [Lanci and Kent, 2006].

- Finally, MSPs have also been suggested to be involved in the formation of Nitric Acid Trihydrate (NAT) particles in polar stratospheric clouds whose existence can otherwise not be explained based on the current knowledge of the relevant thermodynamics [Voigt et al., 2005].

Thus, despite their obvious importance, very little is known about the properties of MSPs and a number of factors associated with the formation of these particles is poorly understood.

This lack of knowledge is mainly due to the complications associated with the measurements at mesospheric altitudes and tiny dimensions and low number densities of the particles, rendering, for example, the detection by optical methods extremely challenging [Rapp et al., 2005; Megner et al., 2008c].

In order to quantify meteor smoke in the mesopause region, detailed knowledge about the meteoroid flux, meteor ablation and recondensation process are required. In the following subsection we consider all these processes in detail and summarize the existing experimental and theoretical achievements.

2.1 The meteoroid flux and its physical characteristics

The meteoroid influx determines the amount of material available for MSPs formation. Hence, the accurate knowledge of the global meteoric input function is critical. This function accounts for the annual and diurnal variations of meteor rates, global distribution, directional-

ity, and velocity and mass distributions. Estimates of most of these parameters are still very uncertain and has to be improved [Janches et al., 2006; Fentzke and Janches, 2008].

The total meteoric mass fluxes entering the Earth's atmosphere derived by different approaches and methods are summarized in Table 2.1. There are some principal methods for

Table 2.1: Diurnal whole-Earth meteoric mass flux estimates

Method	Reference	Mass flux [tons/day]	Mass range covered [g]
Interpolation from satellite and optical data	Hughes [1978]	44	$10^{-13} - 10^{2}$
Hypervelocity impact craters on LDEF satellite	Love and Brownlee [1993]	110 ± 55	$10^{-9} - 10^{-4}$
Determines particle masses from ablating meteoriods (HPLA)	Mathews et al. [2001]	4.4 and 7.4	$< 2 \times 10^{-5}$
Lunar microcrater, satellite, radar, optical	Ceplecha et al. [1998]	$66 - 360$	$10^{-21} - 10^{-8}$/ $10^{-21} - 10^{15}$
Single-particle analyses of stratospheric aerosol	Cziczo et al. [2001]	$20 - 100$	$> 2 \times 10^{-7}$
Accumulation of iridium in ocean-floor sediments	Wasson and Kyte [1987]	240	$10^{-14} - 10^{17}$
Determination of Ir and Pt in Greenland Ice core	Gabrielli et al. [2004]	214 ± 82 (uncorrected) 38 ± 14 (corrected)	$> 7.6 \times 10^{-13}$
Modeling Na layer	Plane [2004]	< 20	$10^{-7} - 10^{-4}$

assessing the influx. First, by observing the occurrence rate of meteors, fireballs, meteorite falls and cratering events, and estimating the mass of the causative parent (optical and radar methods). In many of these cases the influx is distributed only locally and not globally. Additionally, average velocity and angle have to be assumed for the interpretation of measurements.

Alternatively, it is possible to collect the material that actually reaches the surface. This is manifested by the unusual iridium content of the dirt locked up in, for example, preindustrial Arctic and Antarctic ice, and in the metallic spherules and the manganese and osmium found in the old sediments at the bottoms of some of the worlds oceans [Hughes, 1997]. These methods involve uncertainties like the terrestrial age dating of meteorites, meteorite catchment area, recovery rate, weathering and differential survival of meteorites, and the removal of meteorites by wind [Zolensky et al., 2006].

Another approach is to estimate the dust influx just before it enters to the Earths atmo-

sphere. The extraterrestrial mass flux was determined by measuring hypervelocity impact craters found on the space-facing collector surfaces on the gravity gradient stabilized *Long Duration Exposure Facility* (LDEF) satellite [Love and Brownlee, 1993]. The LDEF satellite orbited at a height from 331 to 480 km for 5.77 years. On return to Earth, 761 extraterrestrially produced microcraters were found on the 5.6 m^2 surface of the "thermal control panel".

Many other studies have also been made on the microcratered surface of exposed Moon rocks, which were returned to Earth by the Apollo missions. The exposure age of the rocks can be estimated from the damage they have received from cosmic rays, but again, these rocks do not give a measurement of the large body flux. Anything that would smash the rock to pieces is not recorded.

As can be seen from Table 2.1, the daily global amount of meteoric material is still not well defined and the estimates vary by more than an order of magnitude (from ∼7 to 250 tons). The main problem in meteoroid flux estimation is the fact that masses of meteoroids entering the Earth's atmosphere extend over more than 30 orders of magnitude [e.g., von Zahn, 2005]. A large majority of the total meteoric mass flux is however, carried, by meteoroids from 10^{-7} to 10^{-3} g. But even for this limited mass range, it turns out, that there is still no single instrument or any easy way to measure directly the total mass flux to the Earth's upper atmosphere. To arrive at quantitative value of this parameter, one needs to combine information from two, if not more, different observation methods [von Zahn, 2005].

The currently most accepted value of meteoric flux was derived by Hughes [1978] and amounts to 44 tons/day. This figure results from different independent methods: 1) Satellite in-situ measurements by penetration, impact and ionization detectors, 2) ground-based radar observations of meteor-trail echoes, and 3) ground-based visual and camera observation of meteors.

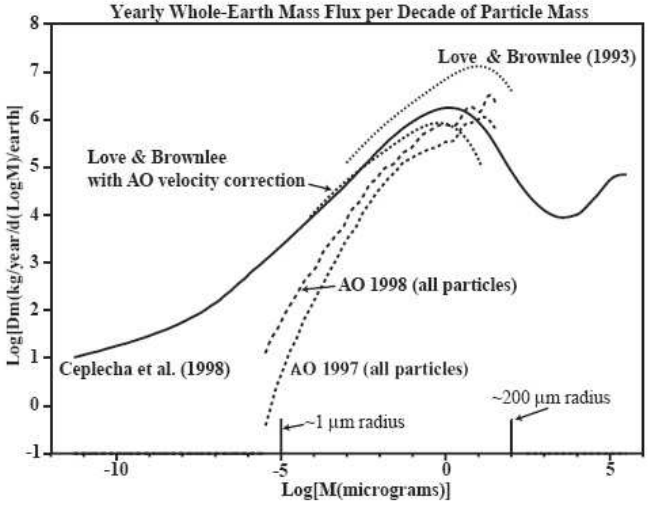

Figure 2.2: Micrometeoroid mass fluxes to the upper atmosphere extended to whole Earth annualized mass fluxes per log differential meteoroid mass interval as derived from Arecibo radar data (dashed lines). The black solid line is results of Ceplecha et al. [1998]. The dotted lines are estimates based on $LDEF$ cratering per Love and Brownlee [1993] corrections to this estimate based on the AO velocity determinations (taken from Mathews et al. [2001]).

The mass distribution of meteoroids (Fig. 2.2) is not known precisely but its maximum is near a meteoroid mass of ∼10 μg, which corresponds to a radius of 100 μm for a density of 2.0 g/cm^3 [e.g., Hunten et al., 1980].

Finally, it is important to consider the geographical variability of the meteoric influx. Recently, Janches et al. [2004] and Singer et al. [2004] reported meteor observation results from the Antarctic and the Arctic and showed that the activity is not symmetric.

The Janches et al. [2006] model, which uses Monte Carlo simulation techniques and includes

an accepted mass flux, predicts fairly accurately the observed diurnal and seasonal trend of the micrometeor influx rate detected by high power large aperture (HPLA) radars in Puerto Rico (Arecibo) and in Perú (Jicamarca) [Janches and ReVelle, 2005; Janches et al., 2006; Fentzke and Janches, 2008].

These studies clearly show that the seasonal and geographical variation of the meteoroid flux must be considered for a reasonable assessment of local sources and measurements obtained under different observing conditions.

In summary, the meteoric influx is not well known and a highly variable function. This implies that the first step of MSP formation, the input, has to be assumed (more in Section 2.3).

The second step, contributing to MSP formation is the ablation process. The ablation determines the part of meteoric influx, which actually remains in the upper atmosphere as metal atoms and molecules. In the next section we summarize our knowledge about this process.

2.2 Ablation

Reaching the atmosphere the meteoroids experience a strong deceleration and an associated heating because of friction with the air molecules. After melting the final stage of ablation is the evaporation from the body and from its fragments. When evaporation starts, temperatures are close to 2500 K. Further temperature increase is negligible because most of the kinetic energy is spent on the ablation (including fragmentation) process itself. The evaporation is the final stage of the majority of the ablated material [Ceplecha et al., 1998]. This evaporated material is the source of the well known metal layers such as the sodium and potassium layer and is routinely monitored by lidar [e.g., Plane, 1991; von Zahn, 2001; Raizada et al., 2004; Jenniskens, 2004].

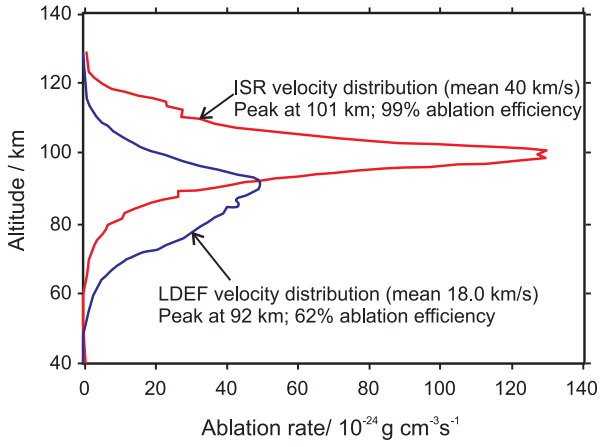

Figure 2.3: Height profiles of the total mass ablation rate for the LDEF meteoroid size distribution (reduced by 85 % in all mass ranges to give a global input of 12.1 t/d), calculated using the assumed LDEF velocity distribution (blue line), or the LDEF velocity distribution shifted by 22 km/s to simulate the velocity distribution observed by incoherent scatter radars (red line) [Plane, 2004].

The altitude at which ablation starts depends on the speed, size, shape, entry angle, and composition of the meteoroids. Faster meteoroids experience stronger deceleration and, therefore, ablate at higher altitudes. The smaller meteoroids are more efficient at radiating the acquired energy and hence can survive a stronger deceleration without the onset of ablation. The very smallest meteoroids never reach the boiling temperature and remain intact throughout the atmosphere. The slowest and the largest meteoroids may not fully evaporate, so that a residual meteorite remains and less material is deposited in the atmosphere [Hunten et al., 1980].

The physics of meteoroid ablation has been modelled by several investigators [Hunten et al., 1980; Love and Brownlee, 1991; McNeil et al., 1998; Kalashnikova et al., 2000; Plane, 2004; Vondrak et al., 2008].

Fig. 2.3 shows the mass ablation rate as

a function of altitude, for the meteoroid mass and velocity distribution estimated from the LDEF experiment [McBride et al., 1999; Plane, 2004]. The peak rate of ablation occurs at 91 km, and about 62 % of the total incoming material vaporizes. This ablation profile is similar in peak height and width to the altitude profile of meteor registrations observed by conventional meteor radars [e.g. Singer et al., 2003, 2004] and by digital ionosonde operated in the frequency range 1-20 MHz [MacDougall and Li, 2001]. Also shown in Fig. 2.3 is the ablation profile predicted for the velocity distribution shifted so that the mean velocity increases from 18 to 40 km/s, which is in line with the high power large aperture (HPLA) radar measurements [Mathews et al., 1997; Janches et al., 2000; Close et al., 2000; Pellinen-Wannberg, 2004]. This ablation profile peaks just above 100 km where 99 % of the material ablates.

It is important to note that the HPLA and conventional meteor radars are two very different techniques based on the detection of two different scattering mechanisms [Janches et al., 2003, 2006]. A radar micrometeor is formed when ionization, caused by the interaction between a micrometeoroid, i.e., micron size particle, and the air molecules, is high enough to be detected by radars. The HPLA is sensitive to so-called head echoes whereas the meteor radar operated mostly in 20-50 MHz frequency range measure the strong Fresnel scattering from the ionization trails [Janches and ReVelle, 2005]. This implies that each technique introduces different biases to the observations, measures different meteoroid populations, and, therefore, needs to be understood separately.

When it comes to a quantitative description of the ablation process it must be realized that a significant number of uncertainties prevail. Among these are the shape of the meteoroids that determines heat conduction and degree of evaporation [Kalashnikova et al., 2000] and the poorly known details of differential ablation [McNeil et al., 2002] determining the predominant species available for MSP formation [e.g., Saunders and Plane, 2006].

Thus, it follows that even though the models of meteor ablation have recently been notably developed, the lack of underlying knowledge about meteoroids makes a direct comparison of the existing measurements and model results extremely difficult. Obviously, all these uncertainties also contribute to the vagueness in the understanding of MSP formation.

2.3 Recondensation of smoke particles

The recondensation of meteor vapor into small particles was first considered by Rosinski and Snow [1961]. They calculated evolution of radially diffusing meteor trail in which the molecules coagulated whenever their Brownian motion caused collision. This model considered the ablation of meteoroids in the range from 12 mg to 48 g with initial velocity of 42 km/sec and ablation altitude of 85 km. Considering vapours in meteor trails, the size distribution of secondary particulate matter was calculated assuming the size of initial smoke particles corresponding to single silicate molecules (0.19 nm). They argued that meteoric materials such as Fe and Si would first be oxidized by colliding with atmospheric O_2 molecules, and would subsequently collide with each other to form larger smoke particles.

The model of Hunten et al. [1980] for the first time estimated altitude distribution of meteoric smoke particles. The calculated dust concentration profiles for mesosphere and stratosphere are shown in Fig. 2.4. The model adapts a discrete phase transition approach and assumes an incoming mass flux of 44 tons/day, an exponential velocity distribution of incoming meteorites, a fixed incoming angle of 37°, and an incoming particle modal mass of 14 μg (118 μm radius). Initial particle sizes were varied between 0.2 and 10 nm, and particles were allowed to evolve by coagulation, sedimentation and eddy diffusion. It was shown that a clear coagulation size spectrum, which is nearly independent of initial size, only develops

below 60 km. This means that the assumption of initial size of smoke particles noticeably influences the obtained results above 60 km.

Megner et al. [2006] show that vertical wind and coagulation efficiency are the two unknowns that have the greatest effect on the smoke distribution. The vertical wind has little influence on the smallest particles but severe effects on the distribution of particles larger than 1 nm radius. The effect of many factors has been shown to be nonlinear.

The transport of MSPs was first quantitatively considered in the model by Megner et al. [2006, 2008a, c], where authors coupled a Hunten et al. [1980] type microphysical model with a two dimensional chemistry-transport model of the atmosphere.

A strong effect of the atmospheric circulation on the global MSP distribution was confirmed by 2-dimensional model of Megner et al. [2008c, a] and 3-dimensional model of Bardeen et al. [2008]. Assuming an initial particle size of 0.2 nm, it was shown that MSPs are efficiently transported away from the summer mesopause to the winter stratosphere.

The effect of the transport is not so apparent on the very small (smaller than 1 nm in radius), short-lived smoke particles, which are produced in situ by meteoric ablation. However, the effect on the nanometer-size MSPs is drastic. The result is a distribution of nanometer sized smoke which is very dependent on latitude and season as shown in Fig 2.5. This is in contrast with the simplistic picture of a homogeneous global meteoric smoke layer, which is currently assumed in many studies of middle atmospheric phenomena, such as noctilucent clouds and PMSE (more in Section 3.1).

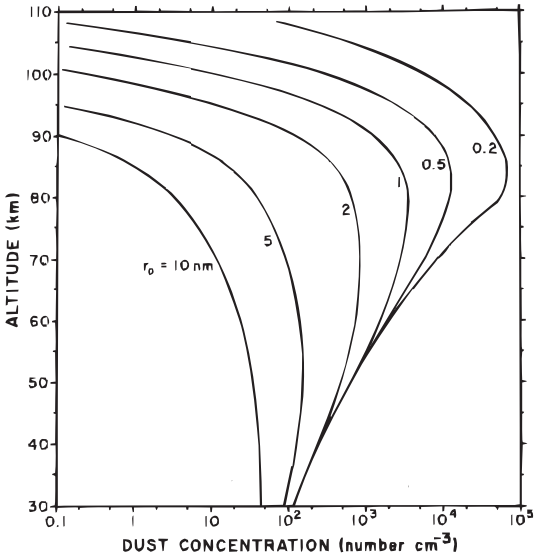

Figure 2.4: Steady-state particle concentration using a dust microphysic model of Hunten et al. [1980]. Concentration profiles are shown for several assumed initial smoke sizes.

In order to understand the physical and chemical processes involved in the formation of meteor smoke, Saunders and Plane [2006] carried out a series of laboratory studies of meteor smoke analogues generation. These authors considered the chemical evolution of Fe and Si atoms created in a meteor trail in the gas phase, to determine the likely species that actually condense to form smoke. It was found, that the iron-containing systems very rapidly form amorphous, fractal, chain-like aggregate structures. Si reacts with O_2 to form SiO and this is, most likely, then oxidized by O_3 to the very stable SiO_2, i.e. silica. In this process spherical compact particles are formed.

Saunders et al. [2007] developed a $1-$dimensional model to describe the formation, growth, and gravitational sedimentation of fractal magnetic particles in the Earth's atmosphere. This model shows that particle concentrations at larger sizes are enhanced in the middle atmosphere when the particles have a fractal (porous) structure compared to spherical (compact) particles.

Thus, the MSPs formation is a very complicated process, which, again, involves a number of uncertainties. In order to constrain the unknown parameters (whose influence, up to now, was only investigated in sensitivity studies), simultaneous measurements of particle properties and background parameters are important. This includes number densities, size distributions, the ratio of charged particles to neutral particles, as well as the determination of the composition

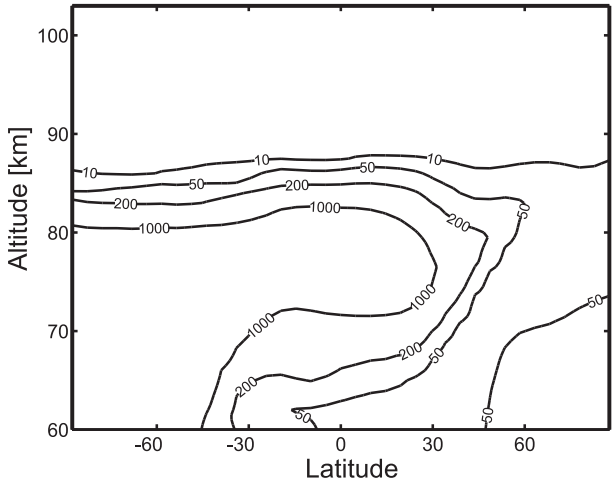

Figure 2.5: Global distribution of meteoric smoke particles larger than 1 nm radius of July $10th$ as obtained by the model of Megner et al. [2008a]. The numbers indicate particles cm^{-3}.

of smoke particles. Knowledge of the composition of meteoric smoke would significantly reduce the uncertainties in both material density and coagulation efficiency [Megner et al., 2006]. Measurements of number densities and size distributions would allow to constrain the factors related to smoke production as long as the atmospheric environment is reasonably well known.

2.4 Measurements of MSPs

It is expected that some part of MSPs is charged, either negatively, by electron capture in the D-region, or positively, by ion capture or by photoemission caused by the solar UV radiation [e.g. Rapp and Lübken, 2001, 1999]. These heavy charged species, i.e., heavier than electrons and molecular ions, can be detected in situ by rocket-borne instruments that utilize both large particles' mass and their charge (see below). Prior to this thesis the measurements of MSPs were only limited to their charged fraction.

An overview of all rocket borne in situ MSP measurements can be found in Rapp et al. [2007] and Amyx et al. [2008] and is summarized in Fig.2.6. The instruments used for charged aerosol measurements are: Gerdien condenser [Croskey et al., 2001; Mitchell et al., 2001], magnetically shielded impact detectors [Horányi et al., 2000; Robertson et al., 2004; Amyx et al., 2008], ion mass spectrometers [Pfeilsticker and Arnold, 1989; Schulte and Arnold, 1992] and Faraday cups with various modifications [Havnes et al., 1996; Gelinas et al., 1998; Lynch et al., 2005; Rapp et al., 2005]. All these instruments measure currents produced by charged mesospheric constituents which are heavier than some minimal detectable limit. There is only one instrument designed for the in-flight collection of MSPs and return to the ground for later analysis in the laboratory [Gumbel et al., 2005; Hedin et al., 2007b], but the analysis of the collected material is still in progress and results are not available yet.

The detection of nanometer sized particles is especially problematic since the shock wave in front of the rocket may prevent small particles from reaching the detector [Horányi et al., 1999; Rapp et al., 2005; Hedin et al., 2007a]. The size cutoff above which particles are detected is a complicated function of the shape of the rocket instrument, the density of the air, the velocity of the rocket, and the properties of the particles. Hence, it is not trivial to estimate the fraction of the MSPs which can be measured with a given instrument and it

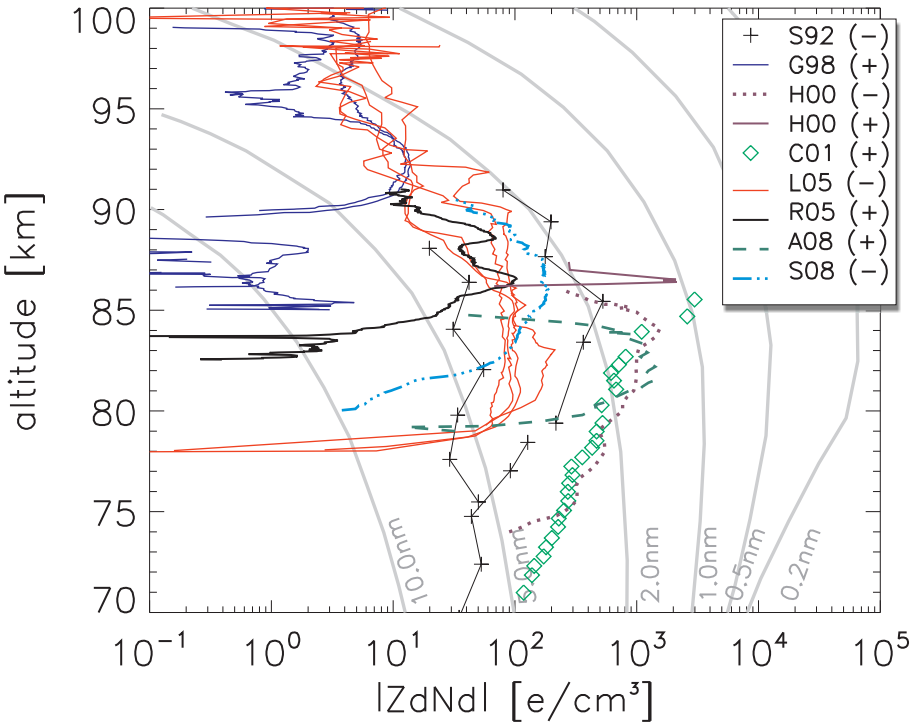

Figure 2.6: Altitude profiles of the charge number densities of mesospheric nano-particles measured in situ with different techniques. To the right of the flight labels, whether positive (+) or negative (−) particles were observed (see Table 2.2 for more details) is indicated . The grey solid lines reproduce calculations of the number densities of MSPs for different initial particle radii (see grey labels) from the work by Hunten et al. [1980]. Note that within the Hunten-theory these lines are roughly equivalent to the cumulative number densities of particles larger than the considered radii (extended Fig. 1 of Rapp et al. [2007]).

varies greatly with altitude. This makes it difficult to produce a direct comparison of all the measurements between each other and with model estimations. An attempt to compare in situ measurements and models taking into account the discussed above issues is presented in Section 5.1 of this thesis.

Moreover, it has generally been assumed that the aerosol particles deposit all their charge onto the collector and leave as neutrals. This assumption is used for the calculation of the density of charged particles. Nevertheless, we need to consider the possibility that the observed charge sign does not reflect the true MSP charge, but that the observed currents are rather caused by secondary effects such as charge production by particle fragmentation or triboelectric charging [Havnes and Naesheim, 2007; Amyx et al., 2008]. These processes are irrelevant for the estimation of number densities as long as each particle produces one elementary charge. But the interpretation of the measurements can differ depending on the physical process that produced the measured current. The other problem is to account for the polarity of the collected charge for the Faraday cups and impact detectors. These instruments measure the net current deposited on the detector by all the impacting particles (both positive and negative). The ion mass spectrometers and Gerdien condensers are sensitive to one polarity of the species. Lynch et al. [2005] developed a detector that allows to distinguish between the negative and positive particles by modulation screen switching between positive and negative 11 V at 1 kHz. This detector has been flown four times (see Table 2.2) and measured negatively charged particles in an altitude range between 78 km and

Table 2.2: Details about previous measurements of charged mesospheric particles (outside areas of noctilucent clouds and polar mesosphere summer echoes)

Label	Latitude	Date	Nr. of payloads	Technique	Charge sign	Reference
S92	$68°N$	03 Aug 82	1	Ion mass spectrometer	$(-)$	Schulte and Arnold [1992]
G98	$18°N$	19 *Feb* 98	1	Faraday cup	$(+)$	Gelinas et al. [1998]
H00	$32°N$	02 *Nov* 98	1	CDD	$(-,+)$	Horányi et al. [2000]
C01	$69°N$	05 *Jul* 99	1	Gerdien condenser	$(+)$	Croskey et al. [2001]
L05	$65°N$	07, 15 *Mar* 02	4	Faraday Cup	$(-)$	Lynch et al. [2005]
R05	$68°N$	28 *Oct* 04	1	Faraday Cup	$(+)$	Rapp et al. [2005]
A08	$68°N$	10 *Jan* 06	1	CDD	$(+)$	Amyx et al. [2008]
S08	$69°N$	08 *Sep* 06	1	Faraday Cup	$(-)$	Strelnikova et al. [2008]

$\sim$95 km altitude. In spite of differences of the instruments and different time and locations of measurements, all of the instrument designs, except the results of Croskey et al. [2001], found layers of charged aerosol particles in the mesosphere. While it can be plausibly argued that the upper border of MSPs is indeed geophysical, the lower boundary has been shown to be an instrumental effect [Rapp et al., 2005; Hedin et al., 2007a; Amyx et al., 2008]. The measured number densities of MSPs vary from few to thousand particles per cm^3. Note that all these instruments are only representative of the charged fraction of MSPs. This produces large uncertainties in estimation of total amount of MSPs.

As can be seen from Table 2.2, until now (the last reported measurement date is 08 *Sep* 2006), only 11 measurements of MSPs have been performed. This statistics is very poor and further measurements are required in order to investigate the seasonal and diurnal variation as well as the latitudinal dependence.

Chapter 3

Ice particles

The polar summer mesopause is the coldest region of the Earth's atmosphere with even average temperatures as low as 130 K. In this extreme environment ice aerosol layers may appear. Large aerosols can be seen from the ground as clouds (referred to as noctilucent clouds, NLC, or polar mesospheric clouds, PMC). Furthermore, the complete ice population modifies the ambient plasma and gives rise to strong radar echoes known as polar mesosphere summer echo (PMSE). Owing to the fact that the properties of these ice clouds strongly depend on the conditions of the background atmosphere, it has been speculated that observations of these phenomena could be used as an indicator for global, long term change in the mesosphere. However, this certainly requires a detailed and robust physical understanding of all the processes which are relevant for the creation and development of these clouds as well as a robust understanding of their effect on their environment.

3.1 NLC/PMSE

Noctilucent clouds (NLC) are conspicuous and fascinating phenomena, being the highest clouds (they form between 80 and 85 km) in Earth's atmosphere. They are very thin (typically 1 to 3 km), like Cirrus Clouds in the tropopause region, but are so faint that they are never visible in the day. NLC are only visible in twilight and occur only in summer time in both hemispheres from about 5 weeks before solstice to 7 weeks afterward and to regions poleward of geographic latitudes of 50° [Thomas, 1991]. It is now commonly accepted that NLC are the direct consequence of the light scattering from small nanometer-sized ice particles [Hervig et al., 2001; Eremenko et al., 2005]. At mean temperatures between ∼130 K at the mesopause and 150 K at 82 km [Lübken, 1999], the relative water vapor content of a few ppmv [e.g., Seele and Hartogh, 1999] leads to a supersaturated gas phase environment where ice particles can nucleate and grow to a visible size. NLC have been studied by visual observations and photography from the ground for many years [Witt, 1969; Avaste et al., 1980; Gadsden, 1982; Romejko et al., 2003]. Since 1989 it has also been possible to observe NLC with ground-based lidars [Hansen et al., 1989; Baumgarten et al., 2008]. Rapp and Thomas [2006] showed that for a typical distribution of mesospheric ice particles (as estimated from a microphysical model) 90 % of the scattering from mesospheric ice particles arises from particle sizes exceeding 30 nm (in UV range) and 36 nm (in the visible range).

NLC are also often associated with PMSE that are strong 2 MHz−1.29 GHz radar echoes from mesospheric electron irregularities. Radio waves are scattered from irregularities in the radar refractive index which, at mesopause altitudes, is solely determined by the electron number density. For efficient scatter, the electron number density must reveal structures at

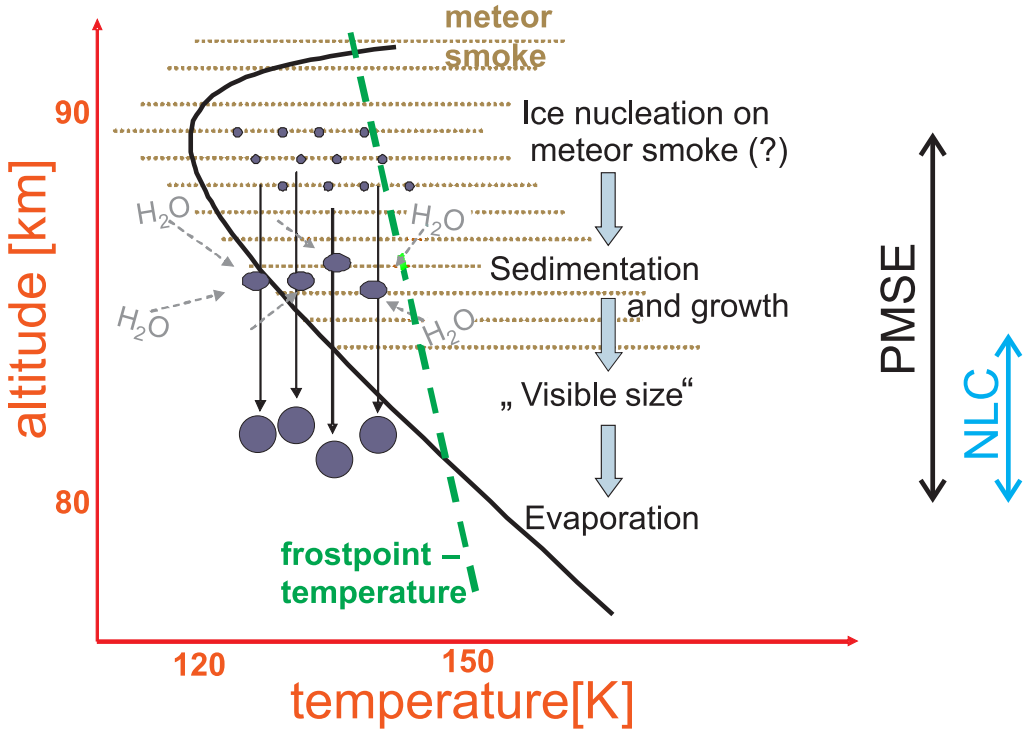

Figure 3.1: Schematic of ice particles building in the summer mesopause region.

the radar half wavelength (Bragg condition; ∼3 m for most VHF radars used for mesosphere soundings). It is now commonly accepted that these structures are ultimately created by neutral air turbulence acting on ambient plasma contains charged nanometer-size ice particles [Rapp and Lübken, 2004]. I.e., in the presence of charged ice particles of nanometer size the electrons are low diffusivity tracers [Kelley et al., 1987; Cho et al., 1992; Rapp and Lübken, 2003]. In such a case, the electrons have a Schmidt number $Sc = \nu/D_e > 1$, where ν is the kinematic viscosity of air and D_e is the electron diffusion coefficient. Batchelor [1959] showed that the energy spectrum of a tracer with a reduced diffusivity reveals a convective-diffusive subrange which extends to much smaller scales as compared to the case with $Sc = 1$.

The general requirement to allow for the observation of structures at VHF and higher frequencies is that the size of charged aerosol particles must be large enough to extend the convective-diffusive subrange of the power spectrum of electrons (by reducing their diffusivity) to a wavelength which is shorter than the Bragg-scale of the probing radar. It is today well established that in the summer polar mesopause region ice particles can grow up to sizes of ∼80 nm [Thomas and McKay, 1985; von Cossart et al., 1999; Baumgarten et al., 2008]. These, in turn, can cause radar echoes at frequencies of up to about 1 GHz [Röttger and La Hoz, 1990; Röttger et al., 1990; Cho and Kelley, 1992; Rapp et al., 2008a].

In summary, the general picture of ice particles growth in the mesosphere is sketched in Fig. 3.1. When the background temperature is lower than the frost point temperature, then ice particles can start to nucleate (low temperatures is necessary but not sufficient condition for ice nucleation). Homogenous nucleation should be negligible, so that pre-existing ice nuclei are required for the formation of ice particles [e.g., Gadsden and Schröder, 1989; Rapp and Thomas, 2006]. Once having formed, the ice particles then grow by the direct deposition of water vapor onto their surface. They settle due to gravity and consume the available water vapor on their way through the atmosphere. During this motion, the particles are further

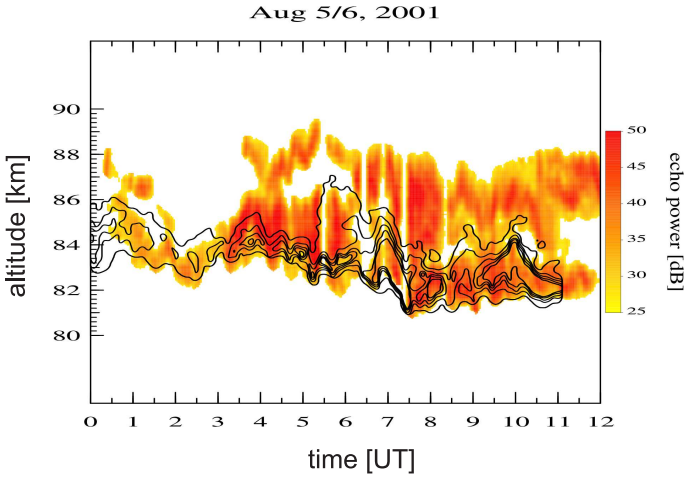

Figure 3.2: Common volume measurement of PMSE and NLC on 5/6 August 2001 at Spitsbergen. The radar echo power above noise is shown in dB (color contour). The backscatter ratios measured by the K lidar are shown in the (unlabeled) black contour lines. This figure is taken from Lübken et al. [2004]

subject to transport by mean winds (vertical and horizontal), and small scale motions, i.e., waves and turbulence. At some size the ice particle can influence backscattered radar signal (for radars with larger frequency, larger particles required to provide PMSE event) [see e.g. Rapp et al., 2008a]. Also, PMSE is not only a function of particle size, as it was introduced above. Both neutral turbulence and sufficient background ionization are required for the creation of PMSE [Lübken et al., 2002; Rapp et al., 2002a]. Schematically the altitude of PMSE observations is sketched as a black arrow on the right-hand-side of Fig. 3.1. This is the whole altitude range where ice particles can exist. Once particles have reached the sizes (equivalent spherical radii) in excess of ∼30 nm, they efficiently scatter light such that they may eventually be observed optically by ground-based or space borne optical instruments. This altitude range is sketched in Fig. 3.1 by the blue arrow. If ice particles grow further, they sediment out of the cold mesopause region and start to evaporate and become invisible for radars and lidars. One of the most compelling observations supporting this physical picture, is frequent coincidence of lower edges of PMSE and NLC [von Zahn and Bremer, 1999; Lübken et al., 2004]. An example of such measurements is shown in Fig. 3.2.

3.2 The nucleation of mesospheric ice particles: state of current understanding

A recent review of microphysics of mesospheric ice particles can be found in Rapp and Thomas [2006]. In this section we briefly summarize the main results presented in that work and discuss a new approach proposed by Megner et al. [2008a].

It is important to note that the homogeneous nucleation of ice particles in the mesosphere is not possible because it exhibits a Gibbs free energy barrier that cannot be overcome under typical conditions at the polar summer mesopause [Witt, 1969]. Thus, under usual mesospheric conditions nucleation requires the existence of some kind of condensation nucleus of approximately 1 nm radius (i.e., critical radius) or larger. Rapp and Thomas [2006] reexamined the possible preexisting nuclei: Large proton hydrate ion clusters, soot (elemental carbon) particles electrophoretically lifted into the mesosphere, sulfuric acid aerosol parti-

cles, sodium bicarbonate, sodium hydroxide, and meteoric smoke particles. To date even the largest observed proton hydrate ion clusters are too small to serve as stable ice nuclei. It appears that ionic nucleation is only feasible under certain extreme atmospheric conditions and probably only plays a minor role in the nucleation of mesospheric ice particles [Gumbel et al., 2003]. For the existence of soot particles, sulfuric acid aerosol particles, sodium bicarbonate, and sodium hydroxide in the mesopause region there is no experimental evidence. Hence, meteoric smoke particles have long been considered as the most likely candidate for the nuclei of mesospheric ice particles. The existence of these particles in mesospheric altitudes was confirmed by in situ measurements of their charged fraction with radii larger than $\sim$2 nm [Schulte and Arnold, 1992; Gelinas et al., 1998; Lynch et al., 2005; Rapp et al., 2005]. As described in Section 2, under the common assumptions, 1-D studies result in number densities of nanometer-size particles on the order of thousands per cubic centimeter at the mesopause (see Fig. 2.4 and Megner et al. [2008c], their Figs. 2 and 5). A recent 2-dimensional model study, which includes the residual circulation from the summer to the winter pole, however, suggests much lower number densities at the summer mesopause (Fig. 2.5): As few as 10 particles per cubic centimeter with radii larger than 1 nm are left at the summer polar mesopause. Such amount of available nuclei for ice particles growth is contrasting with typical ice number densities of up to several thousands per cm^3 and implies that ice nucleation on neutral MSPs could not account for the total observed ice population.

However, Megner et al. [2008c] suggested that negatively charged meteoric smoke particles may solve this dilemma. Charged particles in combination with temperature fluctuations due to gravity waves offer another possible solution. Such fluctuations in the mesopause region were measured to vary around 10 K [Rapp et al., 2002b]. If the particles are charged, the potential barrier of the Gibbs potential disappears typically below $125-130$ K, so that the critical radius no longer exists, and particles, even smaller than 1 nm, may act as condensation nuclei. Ice can then start to grow on these nuclei during the temperature minimum, so that when the temperature rises, they are already larger than 1 nm and thus stable growth can continue.

To verify these hypotheses, combined measurements of charged and uncharged smoke particles together with a characterization of ionospheric and thermal background conditions are required.

3.3 Measurements of ice particles in the mesopause region

Large mesospheric ice particles can be observed as noctilucent clouds (NLC). The clouds can be visually observed during twilight when the sun is below the horizon but still illuminates mesosphere. Since the first days of NLC discovery and up to now, visual and photographical observations are an effective method for systematic NLC studies [Witt, 1969; Avaste et al., 1980; Gadsden, 1982; Romejko et al., 2003]. The spatial morphology as well as the horizontal structure of NLC on continental as well as small scales is observed by combination of the photos from different cameras. Also by simultaneous photographs taken at two or more adequately separated stations, the height of clouds can be determined [Jesse, 1887; Avaste et al., 1980; Gadsden, 1982, 1998]. The longest measurement up to now is visual observations of the NLC frequency and coverage of $\sim$40 years [Romejko et al., 2003]. Though such measurements yield morphology of the ice clouds, they do not allow to infer a more detailed information about ice particles.

As from the ground, NLC can also be optically observed from space [DeLand et al., 2006]. An important factor in optical analysis is the extreme sensitivity of scattered light intensity to the particles radius r, which varies as r^6 for the bulk distribution. Also, when interpreting

the results from remote soundings of NLC it has to be taken into account that the instruments always observe an ensemble of particles [e.g., Baumgarten et al., 2008].

Apart from some NLC observations of rather weird optical signatures [Alpers et al., 2001; Carbary et al., 2004], deduced radii generally agree with each other [Hervig et al., 2001; von Savigny et al., 2005; Karlsson and Rapp, 2006; Baumgarten et al., 2007, 2008] and fall close to the r = 50 nm "*standard*" established by Thomas and McKay [1985] and Rusch et al. [1991]. This standard, obtained under the assumption of a fixed distribution width from microphysical modelling, was proven to hold even without this assumption von Cossart et al. [1999] and was recently confirmed by Baumgarten et al. [2008] who could rely on a greatly improved statistics.

Recent analysis of Solar Occultation For Ice Experiment (SOFIE) onboard the Aeronomy of Ice in the Mesosphere (AIM) spacecraft shows lower values [Hervig et al., 2008b, a]. SOFIE yields effective radii that are generally consistent with concurrent ALOMAR lidar measurements, although SOFIE indicates effective radii from 5 to 15 nm that are not observed by the lidar. The comparison of ice mass densities (M_{ice}) also shows lower values for SOFIE. Thus, M_{ice} measured by the SOFIE instrument ranges from 0.1 to 80 ng m^{-3}, whereas all other measurements and models indicate 1-286 ng m^{-3} [von Cossart et al., 1999; von Savigny et al., 2005; Rapp and Thomas, 2006; Baumgarten et al., 2007, 2008]. This difference is consistent with greater sensitivity of the SOFIE instrument compared to previous instruments, but is also due to averaging by SOFIE over a relatively large sampling volume.

Direct measurements of ice particles sizes and number densities by radar technique were not possible until the work of Strelnikova et al. [2007]. That was the first estimate of the particles' sizes from radar observations of a PMSE event that was done in the frame of this thesis. Corresponding results are discussed in Section 5.3.

NLC particle properties have also been investigated in situ by scattering light photometry and by particle impact probes [Gumbel and Witt, 1998]. A review of photometric investigation can be found in Thomas and McKay [1985]. The ice particles sizes obtained by this method vary from ∼20 to 300 nm [Thomas and McKay, 1985; Gumbel et al., 2001]. Electrostatic impact detectors, used for measurements of MSPs (Section 2.4) are also employed for NLC studies. This type of detectors aims to measure number densities of heavy charged components. Typical number densities obtained by such measurements vary from some hundreds to many thousands per cubic centimeter [Havnes et al., 1996; Gumbel and Witt, 1998; Blix, 1999; Croskey et al., 2001; Gumbel et al., 2001; Smiley et al., 2003; Rapp et al., 2008b].

Attempts of direct sampling of ice crystals from NLC are reported by Hemenway and Witt [1963]; Farlow et al. [1970]; Rauser and Fechtig [1972]; Hallgren et al. [1973] and others. These measurements, however, were generally regarded as being unreliable because of contamination effects and were not repeatable so far [Gadsden and Schröder, 1989].

Chapter 4

Open questions and objectives of the thesis

Based on our current knowledge described above, the following questions were identified as some of the prime open issues regarding aerosols in the MLT region.

✓ One of the main problems is the lack of knowledge on MSPs' properties like number density and size distribution that are important for understanding of various mesospheric phenomena.

Reliable measurements of MSP's properties are required in order to verify the existing models. Unfortunately, the few existing measurements, summarized in Section 2.4, are not conclusive and, certainly, do not provide sufficient information for such verification. Moreover, these measurements include large uncertainties. Factors contributing to the uncertainties are inefficient instrumental sensitivities, on the one hand, and, on the other hand the limitation that only the charged MSP can be detected.

✓ Another open question is the variability of MSPs. Models predict highly variable number densities of MSPs (see Section 2.3) that certainly needs to be experimentally verified. To study dynamical processes connected to the MSPs it is necessary to conduct continuous observations, which is in contrast to the rocket-borne instant measurements−the only ones available prior to this work.

✓ Continuous observations of charged aerosols in the mesosphere are also important for PMSE studies. While such important parameters as turbulence and electron density can be measured from the ground, measurements of charged aerosols were so far only performed using in situ techniques. While the radars and, in particular, the ISR, among the other advantages like unpretentiousness to the weather conditions, are capable of measuring different parameters simultaneously they have not been used to characterize charged aerosols particles.

✓ MSPs as nuclei for the formation of the ice particle is still a hypothesis that have yet to be confirmed experimentally.

The objectives of the thesis are, therefore, defined as follows:

1. The first objective is development and application of a new instrument, that allows to measure both neutral and charged MSPs and is sufficiently sensitive to measure all (even very tiny) particles. Such a new instrument can then yield information about the total amount of MSPs that can, in turn, be compared with model results. Furthermore, information about the charged fraction of MSPs can be used for comparison with other measurements (it is necessary to understand the variability) and for charge balance modelling.

2. The second objective is development and application of a new measurement technique that allows to perform continuous observations of the mesospheric aerosols (either MSPs or ice particles). Taking into account the amount of data available today from modern radar systems, such a technique can significantly extend the observational data base and, therefor, will make it possible to produce meaningful statistical analysis of the aerosol properties and their relation to the mesospheric phenomena.

The first goal was addressed during the work on the still continuing ECOMA project. The project has already yielded new geophysical findings that are discussed in papers I-III and summarized in Section 5.1.

To reach the goal of continuous soundings, a new ground-based technique for measurements of MSP properties using incoherent scatter radar (ISR) was developed. This new technique and first results are described in papers IV-VI and summarized in Section 5.2.

Chapter 5

Results

5.1 The ECOMA particle detector

The new particle detector is a combination of a Faraday-cup and a xenon-flashlamp for the photo-ionization of meteor dust particles (Fig. 5.1).

The design of the Faraday cup comprises a collecting electrode (held at the payload potential by a negative feedback loop of the electrometer) for the measurement of charged particles and two grids (biased at ±3-6 V relative to payload potential) to shield the collector against electrons and ions. This classical design of the Faraday Cup is combined with a xenon-flashlamp (in the center of the cup) which emits UV-photons for the active photoionization of particles. The flash lamp is operated at a repetition rate of 20 Hz.

Briefly this technique can be summarized as follows. Directly after the flash photoelectrons are emitted from MSPs in all directions (solid angle of 4π sr). The volume where the ionization rate is larger than ∼1 % only extends to about 1 m ahead of the detector because of the beam divergence. Additionally, the probability of the electron to hit the detector's electrode decreases with the distance. Thus, the electrons released from the MSPs after the flash originate from the conically shaped nearby volume with an opening angle of 30° and can be measured as a current. Because of the high electron velocity, the response on the flashing is shorter than 50 μs with the maximum during the first 10 μs.

The sensitive electrometer has two measurement channels with sampling rates of 1 and 100 kHz. This corresponds to the classical Faraday Cup and the new measurement technique, respectively.

The 100 kHz channel yields information about the total particle number density multi-

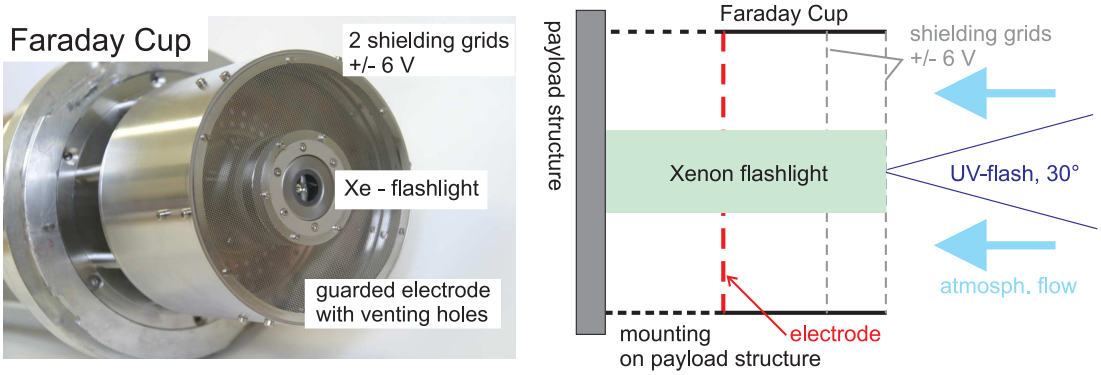

Figure 5.1: Photo and schematic of the ECOMA-particle detector.

plied by particles cross section. For the interpretation of these measurements an additional modelling is required. This new measurement technique is discussed in detail in **Paper I** where the relation between MSPs' number density, their cross section, and measured current is introduced. It was shown that currents detected below ∼90 km height are due to photoionization of MSPs since other potential contributions from species with low work function create currents that are orders of magnitude smaller.

The 1 kHz channel (classical Faraday Cup) obtains 64 samples between two subsequent flashes. Because the duration of the flash-produced photocurrent is shorter than the time sampling interval of this channel (1 ms), only the first sample after the flash measurement point is affected by the photoelectrons. During the next 63 samples the electrometer measures the net natural charge of the particles (either negative or positive), if there is any. Hence, the measurements by this channel yield the information about the number density of charged fraction of the meteor smoke particles. This current can be compared with other measurements provided by the similar instruments (see Table 2.2 and Fig. 2.6).

5.1.1 Measurements of MSPs by classical Faraday Cup

As described above, the 1 kHz channel of the ECOMA particle detector represents the classical Faraday cup measurements.

For the first time this detector was used in October 28, 2004 at 21 : 49 LT from Kiruna ($68°N,\ 21°E$), Sweden, under nighttime conditions. The results are reported by Rapp et al. [2005]. The measurements show a positive current between ∼82 and 90 km with a maximum of +25 pA at 86 km. In the summary plot (Fig. 2.6) this measured altitude profile is shown as black line and labelled as "R05". Qualitatively, these measurements agree well with four flights of Lynch et al. [2005] in the altitude range between 85 and 90 km. An aerodynamical analysis of the particle sampling efficiency for our instrument above 80 km reveals that the observed particles must have been larger than ∼2 nm assuming spherical particles with a mass density of 3 g/cm^3. Below 80 km the minimum detectable radius rapidly increases with the altitude decrease. Thus, the cut-off below ∼84 km (Fig. 2.6, R05) is due to the aerodynamics. I.e., the shock wave in front of the supersonically moving rocket prevents the smallest particles from reaching the detector's interior and, hence, defines an altitude-dependent sensitivity of the instrument. We conclude that the discrepancy in the altitude of the lower edge of the measured layers obtained by the similar instruments, but by the different investigators (G98, L05, R05, and S08 in Fig. 2.6) can well be explained by the different geometry (and, therefore, aerodynamics) of the detectors.

The next measurement was done in the frame of the ECOMA campaign (Existence and charge state of meteor smoke particles in the middle atmosphere) conducted from the North-Norwegian Andøya Rocket Range (69 °N) in September 8, 2006 at 22:17:00 UT (ECOMA01). The results of this flight discussed in detail in **Paper II**. The measurements of charged component show a layer of the negatively charged particles between 80 and 90 km (red line in Fig. 5.2 and S08 in Fig. 2.6).

Comparison of the first two flights of the ECOMA particle detector shows the existence of MSP layers between ∼80 and 90 km with the different polarity. Thus, using the same instrument under nearly the same conditions we observed smoke particles of the different sign. In Paper II we discuss all possibilities that can produce this difference. Briefly, there are two possible solutions for this problem. The first is that the measured current was due to the charge transfer from the charged dust particles to the electrode, that is the instrument worked as supposed. The second interpretation of this difference in sign is that triboelectric charging prevailed in one of these flights. The triboelectric charging can appear if electrode

and impacting dust particle have different work functions [Amyx et al., 2008]. To solve this dilemma further measurements are required.

5.1.2 Measurements of meteoric dust by active photoionization

The first rocket sounding using the new method for MSPs detection by active photoionization was done on September 8, 2006 at 22:17:00 UT (ECOMA01).

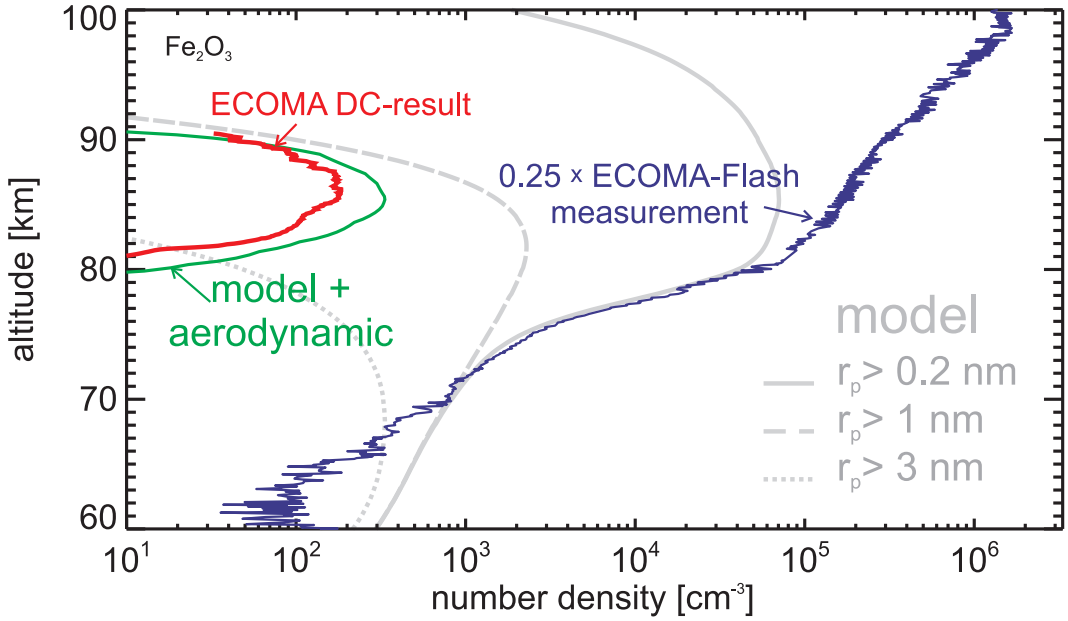

Figure 5.2: Results obtained during ECOMA01 campaign. The red and blue curves show the number densities obtained by 1 and 100 kHz channels respectively. The grey lines show the modeled number densities for different radii. The green line represents the combination of modeled MSPs with aerodynamical model.

The details on this flight are discussed in **Paper II**. The main results are summarized in Fig. 5.2 where the simultaneous measurements of MSPs by two measurement techniques in comparison with the theoretical estimation are presented. To convert the measured flash-current to the number density we assumed that the particles are Fe_2O_3-spheres with quantum yield of Y=1.0. The size distribution needed for cross section estimation was taken from the model of Megner et al. [2006].

The flash method (100 kHz channel), which measures the entire MSP population, observed a broad altitudinal dust distribution, i.e. from 60 to ~90 km (Fig. 5.2, blue line). Whereas the 1 kHz channel only measured a layer of the charged dust between 80 to 90 km. Note, that ice particles cannot exist at those heights at the time of the ECOMA01 launch. Fig. 5.2 demonstrates that the *"layering"* observed by the classical Faraday cup technique (1 kHz channel), that is the dust layer confined to the heights 80 to 90 km, is not a geophysical feature but instrumental limitation. This conclusion is also valid for all the other similar dust detectors.

Quantitatively, the measured dust density exceeds the model prediction by a factor of 4. This can be due to underestimation of the photoelectron yield, particle cross section, or meteoroid influx assumed in the model of Megner et al. [2006]. However, qualitatively, the model predictions and the measurements by the flash channel show good agreement. The importance of these measurements is that they were the first experimental confirmation of

the existence of MSPs in the entire height range of the mesosphere.

5.1.3 Measurements of mesospheric aerosols in a PMSE/NLC event

The ECOMA03 sounding rocket was launched on 3 August 2007, at 23:22 UT from the Andøya Rocket Range (69° N). The detailed description of the results obtained during this flight can be found in **Paper III**. The special feature of the ECOMA03 flight is that this was the first flight of the ECOMA instrument under PMSE/NLC conditions.

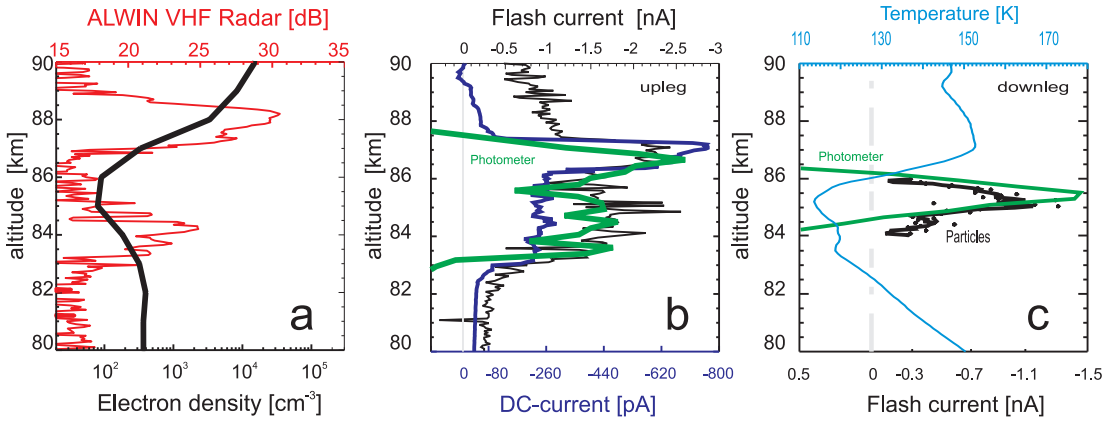

Figure 5.3: Overview of measurements with the ECOMA-particle detector in comparison to **a**: ALWIN VHF-radar measurements of PMSE (red line) and absolute electron densities from the Faraday propagation experiment (black line). **b**: DC- (blue) and Flash- (black) currents measured by the ECOMA-particle detector on upleg compared to photometer measurements indicating the presence of "visible" ice particles (green line), i.e., ice particles with radii in excess of $\gg$20 nm. **c**: the same as **b**-plot, but for downleg. DC-measurements during downleg are impossible because of the wake conditions for the instrument. Also temperature profile measured by the CONE-instrument (sky-blue) is shown.

An overview of the measurements obtained during this flight is shown in Fig. 5.3. In the left panel ALWIN radar measurements with the 7° North-West-beam are shown for the time of the rocket launch. Note that the rocket passed through the edge of the volume illuminated by this beam on the upleg part of the rocket trajectory. In the same panel we show electron density measurements by the Faraday rotation experiment [Friedrich et al., 2009]. Interestingly, this shows that the PMSE disappeared exactly at the altitudes where the electron density was significantly diminished. This is in line with results of a previous study by Rapp et al. [2002a] who showed that PMSE require a minimum ambient electron number density of a few hundreds of electrons/cm^3. Hence, it appears that the decaying D-region ionization was, at least partly, responsible for the decay of the PMSE-layer.

The middle panel of Fig. 5.3 shows the ECOMA measurements for the upleg and, in the right panel, for the downleg. The measurements obtained by the flash channel are shown as black lines. This method allows to measure during both upleg and downleg.

The DC-measurements (the classical Faraday cup, blue line in Fig. 5.3) are only available on the upleg and show a layer of net negatively charged particles in the altitude range 82 to 88 km. The same layer was also detected by the flash method and by NLC photometer of the University of Stockholm for the optical in situ detection of mesospheric ice particles [Gumbel et al., 2001; Megner et al., 2008b]. Comparing the in situ measurements of ice aerosols with the radar PMSE observations, we clearly see that the lower edges of the ice layer and of the

PMSE signal are at the same altitude. The upper edge of PMSE signal is ∼1 km higher than the ice layer. Note that the radar detected a double-layer PMSE structure, i.e. there was no detectable signal between ∼85 and 86.5 km, whereas the ice layer detected by in situ measurements does not change between ∼83 and 86 km. This clearly shows that the presence of charged ice particles alone is not a sufficient condition for the existence of PMSE. Rather, PMSE additionally require a mechanism creating small scale structures at the radar Bragg scale which is commonly assumed to be neutral air turbulence in the presence of charged aerosol particles [e.g. Kelley et al., 1987; Rapp and Lübken, 2004] and sufficient ionization, as suggested by the comparison of the PMSE with the electron densities discussed above.

The measured photoelectron currents are a unique function of the ice particle volume density (and hence ice mass) within an uncertainty of only 15 % and the derived values are in the range $2-8\times10^{-14}\ cm^3/cm^3$ and are in general agreement with independent estimates from either satellite instruments [Hervig et al., 2008a, b] or lidar measurements [Baumgarten et al., 2007, 2008] even though we note that our values are somewhat at the large side of those previous observations.

Another novelty of these measurements is the capability to deduce, in addition to number densities, also the particles' sizes. This is possible because the DC-current is a function of the number density of the charged aerosols and the flash-current is a function of both number density and cross section of the aerosols. For the estimation of the particles' radii we assume that all the ice particles carry one single charge and are large enough to penetrate inside our detector ($>$ 2 nm). Resulting radii and density values are in the ranges of 20-40 nm and 400-1400 cm^3, respectively.

The downleg data (Fig. 5.3c) show only a thin layer of ice particles between ∼84 and 86 km. Note that the ECOMA flash method cannot distinguish between ice and meteoric smoke particles, whereas the photometer is only sensitive to the ice particles. Thus, because of the coexistence of the layers measured by both instruments, we can conclude that the current measured by the ECOMA-flash channel represents the ice particles. The other, although indirect, confirmation that the layer measured by the ECOMA-flash channel is the icy particles is due to overlapping of the temperature minimum measured in the same volume by the CONE instrument (sky-blue line in Fig. 5.3c). The large difference between the upleg and the downleg data, that are ∼50 km spaced, indicates of that the ice cloud was extremely inhomogeneous.

An interesting feature observed during this flight is the low photoelectron current outside the PMSE/NLC layers. The noise level of the 100 kHz channel is ∼300 pA. For comparison, the currents measured during the ECOMA01 flight rise from ∼2 nA at 60 km to ∼15 nA at 70 km and drop to ∼7 nA at 90 km [Rapp and Strelnikova, 2008; Strelnikova et al., 2008]. Thus, the currents from the MSPs measured in September and discussed above were well above the detection limit. During the ECOMA03 flight in August, there was no detectable signal below the ice layers. On upleg above the ice layer the flash current slowly drops to ∼0.5 nA. The downleg data only show a thin layer of ice particles.

The large discrepancy between ECOMA01 and ECOMA03 can be explained by differences either in the underlying MSPs concentration or in the photoelectric properties of the particles. An in-depth analysis of this discrepancy is beyond the scope of this thesis and will be considered in future studies.

5.2 Measuring charged aerosols by means of ISR

5.2.1 Receiving MSPs parameters from the shape of ISR spectra

In order to study the effect of the charged MSPs on the shape of ISR spectra, Cho et al. [1998] generalized Mathews [1978]'s work to the case of n different plasma constituents and by accounting for collisions between charged particles and neutral molecules using the larger value from either the polarization interaction model or the hard-sphere collision model [Banks and Kockarts, 1973; Schunk, 1975].

The presence of charged MSPs creates a narrow central line superposed on the broad Lorentzian background of the ISR spectrum which is (in the D-region) due to the presence of highly damped ion acoustic waves [Dougherty and Farley, 1963; Tanenbaum, 1968; Mathews, 1978]. This additional narrow line is a consequence of a second diffusion mode in the plasma due to Coulomb coupling between the electrons and charged MSPs [see Cho et al., 1998, for more details].

In this work we applied a new theory of Cho et al. [1998] to data measured by the EISCAT and Arecibo radars [e.g., Folkestad et al., 1983; Janches et al., 2006]. A new algorithm to infer information on the properties of the charged MSPs from the shape of the ISR spectra was developed.

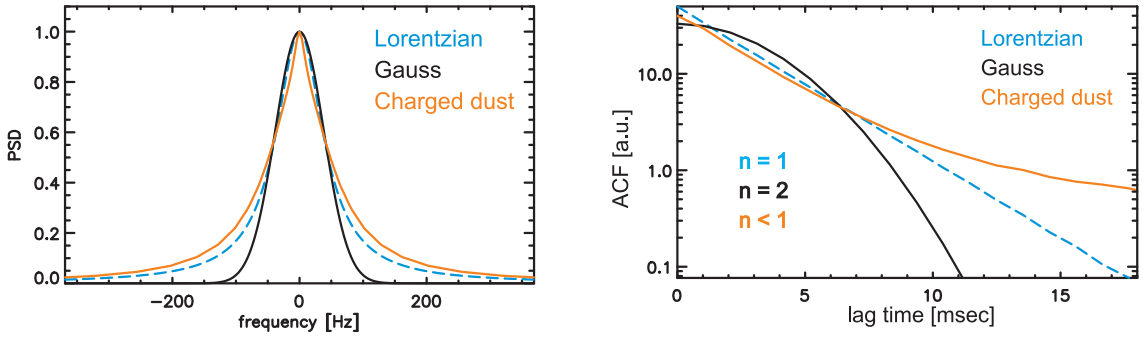

Figure 5.4: Left panel: different types of spectra. Black line is Gaussian, Blue dashed line is Lorentzian, red line is spectra of IS signal in the presence of charged dust particles. The right panel shows the autocorrelation functions for the same three types of spectra.

The first step to infer the information about MSPs from measured spectra was done in **Paper IV**. For our analysis we use the autocorrelation function, which, by definition, is the Fourier transform of the power spectral density. The complex autocorrelation function (ACF) can be written in terms of magnitude and phase. Further below we only deal with the magnitude, ACF, since it yields information about the spectral shape and it reads [Jackel, 2000; Moorcroft, 2004]:

$$ACF(\tau) = ACF_{\tau=0} \cdot \exp\{-(\tau/\tau_e)^n\} \tag{5.1}$$

where τ is the time lag at which the ACF is evaluated, τ_e is a correlation time of the ACF, and the parameter n describes the shape of the ACF. Lorentzian and Gaussian shapes correspond to n=*1* and n=*2*, respectively, whereas $n < 1$ reflects the presence of charged dust particles [Rapp et al., 2007]. Examples of these ACFs are shown in the right panel of Fig. 5.4.

In Paper IV was shown that if the spectra (or ACFs), influenced by the presence of charged dust, were interpreted under the assumption of a Lorentzian spectral shape (because, e.g., noise would mask an obvious departure from such a shape) and were fitted by the Lorentz

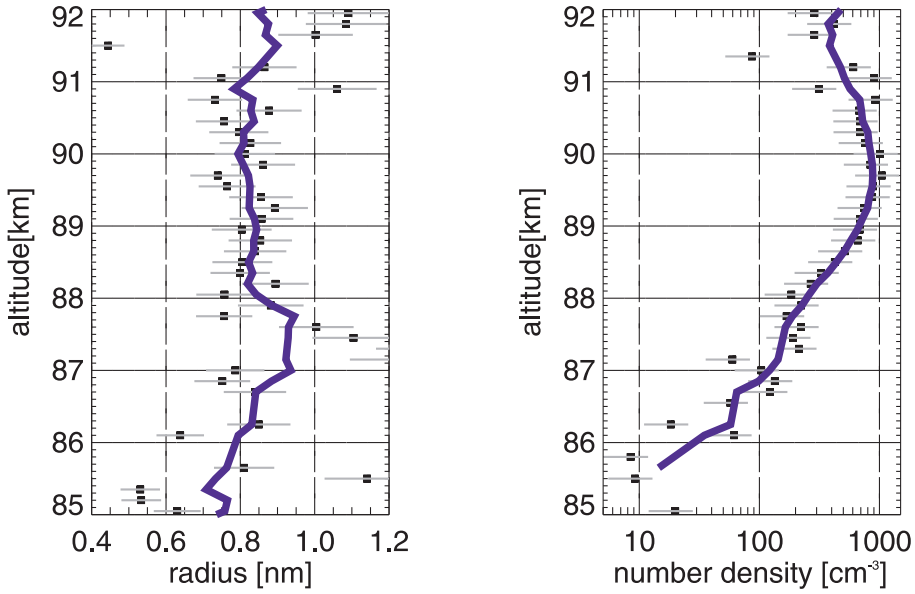

Figure 5.5: Altitude profiles of retrieved radii (left panel) and number densities (right panel) of charged meteor smoke particles. The blue lines are 3-point running means of the original data.

function, then this results in an underestimate of the spectral width as compared to the expectations from classical theory. This corresponds well with the results of previous experimental analyzes by Hansen et al. [1991] and Rietveld and Collis [1993] who found that observed ISR spectra were on average ∼20 % too narrow when compared to theoretical results derived from the classical ISR theory.

Paper V describes a new algorithm with which MSPs number densities and radii can be inferred from ISR spectra and corresponding ACFs. This algorithm is applied to data obtained with the Arecibo radar in September 2006 and the first profiles of MSP number densities and radii derived from ground based observations are presented (also shown in Fig. 5.5). It was shown, that for the cases with charged MSPs the corresponding ACFs can be approximated as the sum of two exponential decays where the first term describes interaction of electrons and positive ions and the second term accounts for the interaction of electrons and charged MSPs. Thus, the time decay (or spectral with) of the second term contains information about the size of MSPs. The larger the particles in sounding volume are, the narrower is the additional line in the spectra (longer correlation time of ACF, see Fig. 2 and 3 in Paper IV).

The more complicated question is the receiving of number densities of MSPs from the measurements. In Paper V only positively charged particles were considered. From the theory of incoherent scattering (IS) it is known that the zero lag of ACF (area under the spectrum) is proportional to the electron number density. Assuming charge neutrality, by analogy, we suggest that the amplitude of the term of ACF that describes the ion-electron interaction is proportional to the ion number density. Correspondingly, the amplitude of the second term is proportional to the number density of positively charged particles. Thus, if the absolute electron number density was measured then one can infer the number density of MSPs from the amplitudes ratio. Using this method we obtained altitude profiles of number densities and radii with values ranging from ∼10 cm^{-3} to ∼1000 cm^{-3} and 0.8 to 1.0 nm, respectively, which fall well within the range of values suggested from independent in situ observations and

model simulations [Rapp et al., 2005; Gelinas et al., 2005; Megner et al., 2006; Strelnikova et al., 2007; Amyx et al., 2008]. These are the first ground-based measurements of MSPs. This new method provides possibility to researches to make continuous measurements and study annual and diurnal variability of MSPs.

In **Paper VI** we show that ACFs, measured by the EISCAT UHF radar have a similar behavior, indicating the presence of charged particles. Assuming that the MSP particles have the distribution function described in Rapp and Thomas [2006], our results agree with model prediction of Hunten et al. [1980].

5.3 PMSE study by ISR technique

As described in Sec. 3.1, PMSE are caused by coherent structures that have a characteristic size equal to the Bragg scale (i.e. half of the wavelength) of the probing radio signal. These structures are created by neutral air turbulence. In the presence of nanometer-size charged ice particles the electrons are low diffusivity tracers [Kelley et al., 1987; Cho et al., 1992; Rapp and Lübken, 2003; Rapp et al., 2008a]. For such tracers it has long been known from the studies of Batchelor [1959] that their power spectrum extends to much smaller scales than the spectrum of the turbulent velocity field itself. This happens because the shear at the smallest existing scales in the velocity field leads to a deformation of the tracer distribution which is not (or not sufficiently) counteracted by molecular diffusion.

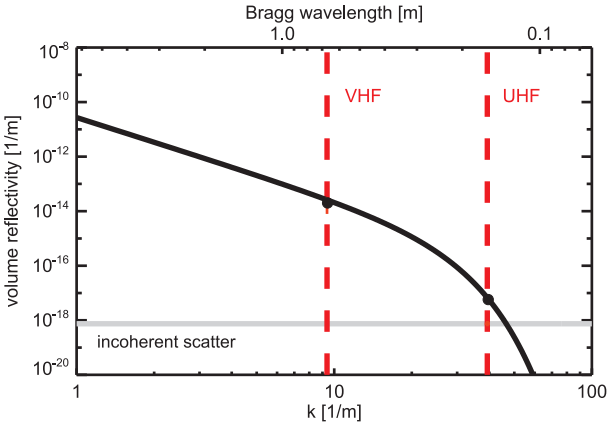

Figure 5.6: The sketch of volume reflectivity assuming typical conditions in the D-region at 85 km, obtained by standard theory, summarized in Rapp and Lübken [2004]. Grey horizontal line shows IS level for electron density of $1.5 * 10^{10}$ m^{-3}

The general requirement to allow for the observation of structures at VHF and higher frequencies is that the dust size/charge-number density must be large enough to extend the convective-diffusive subrange of the energy spectrum of electrons (by reducing their diffusivity) to the wavelength which is shorter than the Bragg-scale of the probing radar. It is today well established that in the summer polar mesopause region ice particles can grow up to sizes of 80 nm [Thomas and McKay, 1985; von Cossart et al., 1999; Baumgarten et al., 2008]. This, in turn, can cause radar echoes at frequencies of up to ∼1 GHz [Röttger and La Hoz, 1990; Röttger et al., 1990; Cho and Kelley, 1992; Rapp et al., 2008a].

In Fig. 5.6 we show volume reflectivity as a function of Bragg wave number (lower axis) or Bragg wavelength (upper axis) for the case of a turbulence induced power spectrum of electron density fluctuation (with suppressed electron diffusion) for typical conditions near the polar summer mesopause at 85 km (see figure caption for more details). The dashed vertical lines show Bragg scales for EISCAT VHF and UHF radars as indicated in the plot. The level of the comparably weak incoherent scattering is marked by the grey horizontal line. The level of the coherent backscattered signal is well above the IS level for the lower frequencies (smaller Bragg wave numbers), but rapidly decrease for higher frequencies (larger Bragg wave numbers).

In this section we summarize results, which confirm the above described theory by two

independent methods.

In **Paper VII** we compared measurements of radar volume reflectivities under PMSE conditions at three frequencies, i.e., 53.5, 224, and 930 MHz corresponding to Bragg wavelengths of 2.8, 0.67, and 0.16 m, with the volume reflectivities derived from the standard theory. The observations quantitatively agree with this theory if Schmidt numbers between 2500 and 5000 are assumed. We then show that these Schmidt numbers correspond to ice particles with radii in the range $20 - 30$ nm which is expected to be a typical case in the polar summer mesopause region. This direct comparison of PMSE radar volume reflectivities measured simultaneously at different frequencies requires a detectable PMSE signal also at UHF frequency. Unfortunately, such observations are very rare and there were just a few such measurements conducted to date [see Röttger et al., 1990; Næsheim et al., 2008; Janches et al., 2008].

An additional new approach is based on the spectral shape. As it is schematically shown in Fig. 5.4, different type of spectra can be observed by ISR. **Paper VIII** examines in detail the question: Which process causes the certain spectral shape? We show, that coherent structures, produced by turbulence, backscatter the signal which has a Gaussian shape (Fig. 5.4, black line). The Doppler spectrum of the incoherent scatter in the D-region exhibits a Lorentzian shape (Fig. 5.4, blue line).

The third type of spectra occurs when no coherent backscattering is present, but presence of the charged dust particles in the scattering region creates a new diffusion mode of the plasma due to the Coulomb coupling between the electrons and charged dust [e.g. Cho et al., 1992; Rapp and Lübken, 2003]. This is reflected in the spectral shape of the IS signal as described by Cho et al. [1998]. In this case the spectrum has neither Lorentzian nor Gaussian shape. Lorentzian and Gaussian shapes correspond to *n=1* and *n=2* in Eq. 5.1, respectively, whereas $n < 1$ reflects the presence of charged dust particles [Rapp et al., 2007].

In Paper VIII we used measurements made with the EISCAT VHF and UHF radars at Tromsø ($69°N, 19.2°E$). We show how the shape of D-region ISR spectra is unambiguously defined by the physical process causing the backscatter.

If pure incoherent scattering takes place, i.e. the classical case of the scattering on "free" electrons, then ISR data reveal a Lorentzian spectral shape. If, however, "free" electrons exhibit coherent structures (e.g. owing to turbulence eddies), then the ISR data show Gaussian spectra. Such coherent echoes from turbulent structures occur during PMSE events. Using the parameter $\mathbf{n} = 2$ (Eq. 5.1) as an indication of a coherent scattering process, we show that inside the PMSE layers the coherent echoes are observed, whereas outside the PMSE layer ACF has the Lorentzian shape, as expected for purely incoherent scatter. We also made a statistical study of PMSE measurements covering ∼86 hours of observations (Table A.2). As expected, outside the PMSE layer the Lorentzian shape dominates in the measurements. Inside the PMSE layer the Gaussian shape of the spectrum was identified in most cases.

These statistical results support the point that PMSE is a scattering from the coherent structures. The same effect we also see, for example, inside Polar Mesosphere Winter Echoes (PMWE) [Lübken et al., 2007, their Fig. 7]. Thus, the spectral shape inside a PMSE layer supports our theoretical understanding that the backscattered echo from this region come from turbulent structures.

The expansion of turbulent structures to the smaller scales depends on the size of the ice particles. If larger particles exist ($20-30$ nm), then turbulent scales can be as small as 0.16 m, i.e. they are detectable at UHF frequency [Rapp et al., 2008a]. PMSE signal, measured at UHF frequency also exhibit a Gaussian shape, but PMSE at these frequencies is a very rare event. Typically, the simultaneous measurements at VHF and UHF frequencies show PMSE event in VHF-measurements, but no measurable power increase in UHF. However even in

the absence of PMSE in the UHF data, the UHF radar signal yields information about the processes that take place in the sounding volume (e.g. the spectral width is extremely narrow). In this case there is a narrowing of the ISR spectra due to the presence of charged particles without the presence of turbulent structures. In such a case the ISR spectra reveal neither a pure Lorentzian nor a Gaussian shape but can be described by Eq. 5.1 with $n < 1$. This type of ISR data directly confirm the presence of charged dust particles, which in turn completely confirms the standard theory.

Chapter 6

Summary and outlook

In the frame of the presented thesis the following achievements were made.

A new instrument for the in situ detection of mesospheric aerosols was developed and successfully used during several sounding rocket campaigns. This instrument for the first ever made measurements of the neutral fraction of the MSPs. These measurements showed a broad altitude distribution of the MSPs which is a new finding that was hitherto only predicted by models. This is in contrast to the previously measured results when MSPs were confined to a layer in the mesosphere. We show that this misleading finding is due to the instrumental limitations of the in situ techniques employed for the aerosol observations.

Another new finding obtained by this new rocket-borne instrument is the simultaneous measurements of meteoric smoke and icy particles. These measurements deduced volume density and size of ice particles. Outside the ice layer, the signal expected from MSPs was below the detection limit. The explanation of this low current can be a low MSPs concentration or change in the photoelectric properties of the particles as compared to our measurements in September 2006.

In addition, a new technique for measurements of MSP properties using incoherent scatter radars (ISR) was introduced. This technique was successfully applied to the measurements by Arecibo and EISCAT radars and makes it possible to continuously observe MSPs by ground-based radars.

Finally, two new self-consistent confirmations of the current PMSE theory were presented. They are only based on ground-based radar measurements which was never done before. The first is based on comparison of absolute volume reflectivities measured by different radars and different frequencies. The second connects the spectral shape (or ACF) of the radio signal to the properties of the backscattering media, that is, it directly employs the new measurement technique. We show, that inside the PMSE layer, the scattering occurs from coherent structures. Under certain conditions the presence of heavy charged particles inside the PMSE layer (measured by VHF radar) can also be seen in UHF radar measurements. This finding clearly shows the role of charged aerosols in PMSE formation.

Outlook:

In Sec. 5.1.1 we showed that the measured current produced by naturally charged particles can have different sign under similar background conditions. We cannot exclude that measured current was not due to charge transfer from charged dust particles to the electrode, i.e. due to triboelectric charging. In order to check how this effect (triboelectric charging) may influence our measurements we developed a new instrument in the frame of the REXUS project

(Rocket Experiment for University Students) conducted by the German Space Agency, DLR (Deutsches Zentrum fur Luft- und Raumfahrt). The idea of the new experiment is to employ a Faraday cup with an electrode which is split into four parts, each made of different material (Cu, Au, C, Cr), that is, each part has a different work function. The current from each part of the electrode has to be measured separately. Comparison of these four measurement channels will yield information about the charge state of particles or the work function of the material constituting the dust particles. The rocket launch is planed for March 2009 from the Esrange, Kiruna (Sweden). These measurements can solve the dilemma about the origin of current and clarify the reliability of Faraday cup measurements of charged particles in the middle atmosphere.

The new radar technique introduced in this thesis should now be applied to conduct a significant statistical study of the annual and diurnal cycle of MSPs as well as their latitudinal variation. Corresponding measurements with the Arecibo and EISCAT radars are currently conducted or are under consideration. Also, a reanalysis of existing EISCAT-UHF measurements using this new technique is required.

The measurements with our new in-situ instrument under different conditions are also required in order to get better statistics. These measurements may bring more detailed knowledge about the MSPs' variation because this method is sensitive to the neutral fraction of MSPs. The question why the measured current outside NLC layer during ECOMA03 campaign was under detection limit have to be considered in detail.

Bibliography

Alpers, M., Gerding, M., Höffner, J., and Schneider, J.: Multiwavelength lidar observation of a strange noctilucent cloud at Kühlungsborn (54° N), J. Geophys. Res., 106, 7945–7953, doi:10.1029/2000JD900666, 2001.

Amyx, K., Sternovsky, Z., Knappmiller, S., Robertson, S., Horányi, M., and Gumbel, J.: In-situ measurement of smoke particles in the wintertime polar mesosphere between 80 and 85 km altitude, J. Atmos. Sol. Terr. Phys., 70, 61–70, doi:10.1016/j.jastp.2007.09.013, 2008.

Avaste, O. A., Fedynskij, A. V., Grechko, G. M., Sevast'yanov, V. I., and Willmann, C.: Advances in noctilucent cloud research in the space era., Pure and Appl. Geophys., 118, 528–580, doi:10.1007/BF01586466, 1980.

Banks, P. M. and Kockarts, G.: Aeronomy, Part A, Academic Press, New York, 1973.

Bardeen, C. G., Toon, O. B., Jensen, E. J., Marsh, D. R., and Harvey, V. L.: Numerical simulations of the three-dimensional distribution of meteoric dust in the mesosphere and upper stratosphere, 113, 17 202–+, doi:10.1029/2007JD009515, 2008.

Batchelor, G. K.: Small-scale variation of convected quantities like temperature in a turbulent fluid, J. Fluid Mech., 5, 113–133, 1959.

Baumgarten, G., Fiedler, J., and von Cossart, G.: The size of noctilucent cloud particles above ALOMAR (69N,16E): Optical modeling and method description, Adv. Space Res., 40, 772–784, doi:10.1016/j.asr.2007.01.018, 2007.

Baumgarten, G., Fiedler, J., Lübken, F.-J., and von Cossart, G.: Particle properties and water content of noctilucent clouds and their interannual variation, J. Geophys. Res., doi:10.1029/2007JD008884, *in press*, 2008.

Blix, T. A.: Small scale plasma and charged aerosol variations and their importance for polar mesosphere summer echoes, Adv. Space Res., 24, 537–546, doi:10.1016/S0273-1177(99)00198-2, 1999.

Brekke, A.: Physics of the Upper Polar Atmosphere, John Wiley & Sons, pp. 490. ISBN 0-471-96018-7, 1997.

Carbary, J. F., Morrison, D., and Romick, G. J.: Evidence for bimodal particle distribution from the spectra of polar mesospheric clouds, Geophys. Res. Lett., 31, 13 108–+, doi:10.1029/2004GL020101, 2004.

Ceplecha, Z., Borovička, J., Elford, W. G., Revelle, D. O., Hawkes, R. L., Porubčan, V., and Šimek, M.: Meteor Phenomena and Bodies, Space Sci. Rev., 84, 327–471, doi:10.1023/A:1005069928850, 1998.

Cho, J. Y., Sulzer, M. P., and Kelley, M. C.: Meteoric dust effects on D-region incoherent scatter radar spectra, J. Atmos. Sol. Terr. Phys., 60, 349–357, 1998.

Cho, J. Y. N. and Kelley, M. C.: Enhancement of Thomson scatter by charged aerosols in the polar mesosphere: measurements with a 1.29 GHz radar, Geophys. Res. Lett., 19, 1097–1100, 1992.

Cho, J. Y. N., Hall, T. M., and Kelley, M. C.: On the role of charged aerosols in polar mesosphere summer echoes, J. Geophys. Res., 97, 875–886, 1992.

Close, S., Hunt, S. M., Minardi, M. J., and McKeen, F. M.: Analysis of Perseid meteor head echo data collected using the Advanced Research Projects Agency Long-Range Tracking and Instrumentation Radar (ALTAIR), Radio Sci., 35, 1233–1240, doi: 10.1029/1999RS002277, 2000.

Croskey, C., Mitchell, J., Friedrich, M., Torkar, K., Hoppe, U.-P., and Goldberg, R.: Electrical structure of PMSE and NLC regions during the DROPPS program, Geophys. Res. Lett., 28, 1427–1430, 2001.

Cziczo, D. J., Thomson, D. S., and Murphy, D. M.: Ablation, flux, and atmospheric implications of meteors inferred from stratospheric aerosol, Science, 291, 1772–1775, 2001.

DeLand, M. T., Shettle, E. P., Thomas, G. E., and Olivero, J. J.: A quarter-century of satellite polar mesospheric cloud observations, J. Atmos. Sol. Terr. Phys., 68, 9–29, doi: 10.1016/j.jastp.2005.08.003, 2006.

DeLand, M. T., Shettle, E. P., Thomas, G. E., and Olivero, J. J.: Latitude-dependent long-term variations in polar mesospheric clouds from SBUV version 3 PMC data, J. Geophys. Res., 112, D10315, doi:10.1029/2006JD007857, 2007.

Dougherty, J. P. and Farley, Jr., D. T.: A theory of incoherent scattering of radio waves by a plasma, 3 Scattering in a partly ionized gas, J. Geophys. Res., 68, 5473–+, 1963.

Eremenko, M. N., Zasetsky, S. V. P. A. Y., Karlsson, B., Rinsland, C. P., Llewellyn, E. J., and Sloan, J. J.: Shape and composition of PMC particles derived from satellite remote sensing measurements, Geophys. Res. Lett., 32, L16S06, doi:10.1029/2005GL023013, 2005.

Farlow, N. H., Ferry, G. V., and Blanchard, M. B.: Examination of surfaces exposed to a noctilucent cloud, August 1, 1968., J. Geophys. Res., 75, 6736–6750, doi: 10.1029/JC075i033p06736, 1970.

Fentzke, J. T. and Janches, D.: A semi-empirical model of the contribution from sporadic meteoroid sources on the meteor input function in the MLT observed at Arecibo, J. Geophys. Res., 113, 3304–+, doi:10.1029/2007JA012531, 2008.

Folkestad, K. T., Hagfors, T., and Westerlund, S.: EISCAT: An updated description of technical characteristics and operational capabilities, Radio Sci., 18, 867–879, 1983.

Friedrich, M., Harrich, M., Steiner, R. J., Torkar, K. M., and Lübken, F.-J.: The quiet auroral ionosphere and its neutral background, Adv. Space Res., 33, 943–948, doi: 10.1016/j.asr.2003.08.006, 2004.

Friedrich, M., Torkar, K. M., Singer, W., Strelnikova, I., and Robertson, S.: Signatures of meteoric particles in ionospheric data, Ann. Geophys., accepted, 2009.

Gabrielli, P., Barbante, C., Plane, J. M. C., Varga, A., Hong, S., Cozzi, G., Gasparia, V., Planchon, F. A. M., Cairns, W., Ferrari, C., Crutzen, P., Ceson, P., and Boutron, C. F.: Meteoric smoke fallout over the holocene epoch revealed by iridium and platinum in Greenland ice, Nature, 432, 1011–1014, 2004.

Gadsden, M.: Noctilucent clouds, Space Sci. Rev., 33, 279–334, doi:10.1007/BF00196999, 1982.

Gadsden, M.: The north-west Europe data on noctilucent clouds: a survey., J. Atmos. Terr. Phys., 60, 1163–1174, 1998.

Gadsden, M. and Schröder, W.: Noctilucent clouds, Springer-Verlag, New York, 1989.

Gelinas, L. J., Lynch, K. A., Kelley, M. C., Collins, S., Baker, S., Zhou, Q., and Friedman, J. S.: First observation of meteoritic charged dust in the tropical mesosphere, Geophys. Res. Lett., 25, 4047–4050, doi:10.1029/1998GL900089, 1998.

Gelinas, L. J., Lynch, K. A., Kelley, M. C., Collins, R. L., Widholm, M., MacDonald, E., Ulwick, J., and Mace, P.: Mesospheric charged dust layer: Implications for neutral chemistry, J. Geophys. Res., 110, A01310, doi:10.1029/2004JA010503, 2005.

Gumbel, J. and Witt, G.: In situ measurements of the vertical structure of a noctilucent cloud, Geophys. Res. Lett., 25, 493–496, doi:10.1029/98GL00056, 1998.

Gumbel, J., Stegman, J., Murtagh, D. P., and Witt, G.: Scattering phase functions and particle sizes in noctilucent clouds, Geophys. Res. Lett., 28, 1415–1418, doi:10.1029/2000GL012414, 2001.

Gumbel, J., Siskind, D. E., Witt, G., Torkar, K. M., and Friedrich, M.: Influence of ice particles on the ion chemistry of the polar summer mesosphere, J. Geophys. Res., 108(D8), 8436, doi:10.1029/2002JD002413, 2003.

Gumbel, J., Waldemarsson, T., Giovane, F., Khaplanov, M., Hedin, J., Karlsson, B., Lossow, S., Megner, L., Stegman, J., Fricke, K. H., Blum, U., Voelger, P., Kirkwood, S., Dalin, P., Sternovsky, Z., Robertson, S., Horányi, M., Stroud, R., Siskind, D. E., Meier, R. R., Blum, J., Summers, M., Plane, J. M. C., Mitchell, N. J., and Rapp, M.: The MAGIC rocket campagn: an overview, Proceedings of the 17th ESA Symposium on European Rocket and Balloon Programmes and Related Research, Sandefjord, Norway (ESA SP–590), pp. 139–144, 2005.

Hallgren, D. S., Schmalberger, D. C., and Hemenway, C. L.: Noctilucent cloud sampling by a multi-experiment payload., in: Space Research XIII, vol. 2 of *Space Research*, pp. 1105–1112, 1973.

Hansen, G., Servazi, M., and von Zahn, U.: First detection of a noctilucent clouds by lidar, Geophys. Res. Lett., 16, 1445–1448, 1989.

Hansen, G., Hoppe, U.-P., Turunen, E., and Pollari, P.: Comparison of observed and calculated incoherent scatter spectra from the D-region, Radio Sci., 26, 1153–1164, 1991.

Havnes, O. and Naesheim, L. I.: On the secondary charging effects and structure of mesospheric dust particles impacting on rocket probes, Ann. Geophys., 25, 623–637, 2007.

Havnes, O., Trøim, J., Blix, T., Mortensen, W., Næsheim, L. I., Thrane, E., and Tønnesen, T.: First detection of charged dust particles in the Earth's mesosphere, J. Geophys. Res., 101, 10 839–10 847, 1996.

Hedin, J., Gumbel, J., and Rapp, M.: On the efficiency of rocket-borne particle detection in the mesosphere, ACPD, 7, 1183–1214, 2007a.

Hedin, J., Gumbel, J., Waldemarsson, T., and Giovane, F.: The aerodynamics of the MAGIC meteoric smoke sampler, Adv. Space Res., 40, 818–824, doi:10.1016/j.asr.2007.06.046, 2007b.

Hemenway, C. and Witt, G.: Particle sampling from noctilucent clouds, Nature, 199, 269–270, 1963.

Hervig, M., Thompson, R., McHugh, M., Gordley, L., Russell III, J., and Summers, M.: First confirmation that water ice is the primary component of polar mesospheric clouds, Geophys. Res. Lett., 28, 971–974, 2001.

Hervig, M. E., Gordley, L. L., III, J. M. R., and Bailey, S. M.: SOFIE PMC observations during the northern summer of 2007, J. Atmos. Sol. Terr. Phys., *submitted*, 2008a.

Hervig, M. E., Gordley, L. L., Stevens, M. H., III, J. M. R., Bailey, S. M., and Baumgarten, G.: Interpretation of SOFIE PMC measurements: Cloud identification and derivation of mass density, particle shape, and particle size, J. Atmos. Sol. Terr. Phys., *submitted*, 2008b.

Horányi, M., Gumbel, J., Witt, G., and Robertson, S.: Simulation of rocket-borne particle measurements in the mesosphere, Geophys. Res. Lett., 26, 1537–1540, doi: 10.1029/1999GL900298, 1999.

Horányi, M., Robertson, S., Smiley, B., Gumbel, J., Witt, G., and Walch, B.: Rocket-borne mesospheric measurement of heavy ($m \gg 10$ amu) charge carriers, Geophys. Res. Lett., 27, 3825–3828, doi:10.1029/2000GL011433, 2000.

Hughes, D. W.: Meteors, in Cosmic Dust (ed. McDonnel, J. A. M.), Wiley, Chichester, 1978.

Hughes, D. W.: Meteors and cosmic dust, Endeavour, 21, doi:10.1016/S0160-9327(96)10030-2, 31–35, 1997.

Hunsucker, R. D. and Hargreaves, J. K.: The high-latitude ionosphere and its effects on radio propagation, pp. 638. ISBN 0521330831. Cambridge, UK: Cambridge University Press, 2002.

Hunten, D. M., Turco, R. P., and Toon, O. B.: Smoke and Dust Particles of Meteoric Origin in the Mesosphere and Stratosphere, J. Atmos. Sci., 37, 1342–1357, 1980.

Jackel, B. J.: Characterization of auroral radar power spectra and autocorrelation functions, Radio Sci., 35, 1009–1024, 2000.

Janches, D. and ReVelle, D. O.: Initial altitude of the micrometeor phenomenon: Comparison between Arecibo radar observations and theory, J. Geophys. Res., 110, 8307–+, doi:10.1029/2005JA011022, 2005.

Janches, D., Mathews, J. D., Meisel, D. D., and Zhou, Q.-H.: Micrometeor observations using the Arecibo 430 MHz radar. I. Determination of the ballistic parameter from measured doppler velocity and deceleration results, Icarus, 145, 53–63, doi:10.1006/icar.1999.6330, 2000.

Janches, D., Nolan, M. C., Meisel, D. D., Mathews, J. D., Zhou, Q. H., and Moser, D. E.: On the geocentric micrometeor velocity distribution, J. Geophys. Res., 108, 1222–+, doi: 10.1029/2002JA009789, 2003.

Janches, D., Palo, S. E., Lau, E. M., Avery, S. K., Avery, J. P., de la Peña, S., and Makarov, N. A.: Diurnal and seasonal variability of the meteoric flux at the South Pole measured with radars, Geophys. Res. Lett., 31, 20 807–+, doi:10.1029/2004GL021104, 2004.

Janches, D., Fritts, D. C., Riggin, D. M., Sulzer, M. P., and Gonzales, S.: Gravity wave and momentum fluxes in the mesosphere and lower thermosphere uding 430 MHz dual-beam measurements at Arecibo: 1. Measurements, methods, and gravity waves, J. Geophys. Res., 111, D18107, doi:10.1029/2005JD006882, 2006.

Janches, D., Heinselman, C. J., Chau, J. L., Chandran, A., and Woodman, R.: Modeling the global micrometeor input function in the upper atmosphere observed by high power and large aperture radars, J. Geophys. Res., 111, 7317–+, doi:10.1029/2006JA011628, 2006.

Janches, D., Fritts, D. C., Nicolls, M. J., and Heinselman, C. J.: Observations of D-region structure and atmospheric tides with PFISR during active aurora, J. Atmos. Sol. Terr. Phys., doi:doi:10.1016/j.jastp.2008.08.015, 2008.

Jenniskens, P.: Meteor induced chemistry, ablation products, and dust in the middle and upper atmosphere from optical spectroscopy of meteors, Adv. Space Res., 33, 1444–1454, doi:10.1016/j.asr.2003.05.001, 2004.

Jesse, O.: Die Beobachtung der leuchtenden Wolken, METZ, 4, 179–181, 1887.

Kalashnikova, O., Horányi, M., Thomas, G. E., and Toon, O. B.: Meteoric smoke production in the atmosphere, Geophys. Res. Lett., 27, 3293–3296, 2000.

Karlsson, B. and Rapp, M.: Latitudinal dependence of noctilucent cloud growth, Geophys. Res. Lett., 33, L11812, doi:10.1029/2006GL025805, 2006.

Kelley, M. C., Farley, D. T., and Röttger, J.: The effect of cluster ions on anomalous VHF backscatter from the summer polar mesosphere, Geophys. Res. Lett., 14, 1031–1034, 1987.

Lanci, L. and Kent, D. V.: Meteoric smoke fallout revealed by superparamagnetism in Greenland ice, Geophys. Res. Lett., 33, L13308, doi:10.1029/2006GL026480, 2006.

Lindzen, R. S.: Turbulence and stress owing to gravity wave and tidal breakdown, J. Geophys. Res., 86, 9707–9714, doi:10.1029/JC086iC10p09707, 1981.

Love, S. G. and Brownlee, D. E.: Heating and thermal transformation of micrometeoroids entering the earth's atmosphere, Icarus, 89, 26–43, doi:10.1016/0019-1035(91)90085-8, 1991.

Love, S. G. and Brownlee, D. E.: A direct measurement of the terrestrial mass accretion rate of cosmic dust, Science, 262, 550–553, 1993.

Lübken, F.-J.: Thermal structure of the arctic summer mesosphere, J. Geophys. Res., 104, 9135–9149, doi:10.1029/1999JD900076, 1999.

Lübken, F.-J., Rapp, M., and Hoffmann, P.: Neutral air turbulence and temperatures in the vicinity of polar mesosphere summer echoes, J. Geophys. Res., 107, ACL 9/1–10, doi: 10.1029/2001JD000915, 2002.

Lübken, F.-J., Zecha, M., Höffner, J., and Röttger, J.: Temperatures, polar mesosphere summer echoes, and noctilucent clouds over Spitsbergen (78°N), J. Geophys. Res., 109, D11203, doi:10.1029/2003JD004247, 2004.

Lübken, F.-J., Singer, W., Latteck, R., and Strelnikova, I.: Radar measurements of turbulence, electron densities, and absolute reflectivities during polar mesosphere winter echoes (PMWE), Adv. Space Res., 40, 758–764, doi:10.1016/j.asr.2007.01.015, 2007.

Lynch, K. A., Gelinas, L. J., Kelley, M. C., Collins, R. L., Widholm, M., Rau, D., MacDonald, E., Liu, Y., Ulwick, J., and Mace, P.: Multiple sounding rocket observations of charged dust in the polar winter mesosphere, J. Geophys. Res., 110, A03302, doi:10.1029/2004JA010502, 2005.

MacDougall, J. W. and Li, X.: Meteor observations with a modern digital ionosonde, J. Atmos. Sol. Terr. Phys., 63, 135–141, 2001.

Mathews, J. D.: The effect of negative ions on collision-dominated Thomson scattering, J. Geophys. Res., 83, 505–512, 1978.

Mathews, J. D., Meisel, D. D., Hunter, K. P., Getman, V. S., and Zhou, Q.: Very high resolution studies of micrometeors using the Arecibo 430 MHz radar, Icarus, 126, 157–169, doi:10.1006/icar.1996.5641, 1997.

Mathews, J. D., Janches, D., Meisel, D. D., and Zhou, Q.-H.: The micrometeoroid mass flux into the upper atmosphere: Arecibo results and a comparison with prior estimates, Geophys. Res. Lett., 28, 1929, 2001.

Mathews, J. D., Briczinski, S. J., Meisel, D. D., and Heinselman, C. J.: Radio and Meteor Science Outcomes From Comparisons of Meteor Radar Observations at AMISR Poker Flat, Sondrestrom, and Arecibo, Earth Moon and Planets, 102, 365–372, doi:10.1007/s11038-007-9168-0, 2008.

McBride, N., Green, S. F., and McDonnell, J. A. M.: Meteoroids and small sized debris in low earth orbit and at 1 Au: results of recent modelling, Adv. Space Res., 23, 73–82, 1999.

McNeil, W. J., Lai, S. T., and Murad, E.: Differential ablation of cosmic dust and implications for the relative abundances of atmospheric metals, J. Geophys. Res., 103, 10 899–10 911, doi:10.1029/98JD00282, 1998.

McNeil, W. J., Murad, E., and Plane, J. M. C.: Models of meteoric metals in the atmosphere, pp. 265–+, Meteors in the Earth's atmosphere. Edited by Edmond Murad and Iwan P. Williams. Publisher: Cambridge, UK: Cambridge University Press, 2002., p.265, 2002.

Megner, L., Rapp, M., and Gumbel, J.: Distribution of meteoric smoke - sensitivity to microphysical properties and atmospheric conditions, Atmos. Chem. Phys., 6, 4415–4426, 2006.

Megner, L., Gumbel, J., Rapp, M., and Siskind, D. E.: Reduced meteoric smoke particle density at the summer pole: Implications for mesospheric ice particle nucleation, Adv. Space Res., 41(1), 41–49, doi:10.1016/j.asr.2007.09.006, 2008a.

Megner, L., Khaplanov, M., Baumgarten, G., and Gumbel, J.: Particle size retrieval from noctilucent clouds at exceptionally high altitudes, Ann. Geophys., subm., 2008b.

Megner, L., Siskind, D. E., Rapp, M., and Gumbel, J.: Global and temporal distribution of meteoric smoke: A two-dimensional simulation study, J. Geophys. Res., 113, 3202–+, doi:10.1029/2007JD009054, 2008c.

Mitchell, J. D., Croskey, C. L., and Goldberg, R. A.: The electrical environment of PMSE/NLC regions: recent measurement results from the DROPPS program, in: European Rocket and Balloon Programmes and Related Research, edited by Warmbein, B., vol. 471 of *ESA Special Publication*, pp. 165–170, 2001.

Moorcroft, D. R.: The shape of auroral backscatter spectra, Geophys. Res. Lett., 31, 9802–+, doi:10.1029/2003GL019340, 2004.

Næsheim, L. I., Havnes, O., and La Hoz, C.: A comparison of polar mesosphere summer echo at VHF (224 MHz) and UHF (930 MHz) and the effects of artificial electron heating, J. Geophys. Res., 113, 8205–+, doi:10.1029/2007JD009245, 2008.

Pellinen-Wannberg, A.: The EISCAT meteor-head method a review and recent observations, Atmos. Chem. Phys., 4, 649–655, 2004.

Pfeilsticker, K. and Arnold, F.: First ion composition measurement in the stratopause region, using a rocket-borne parachute drop sonde, Planet. Space Sci., 37, 315–328, doi: 10.1016/0032-0633(89)90029-9, 1989.

Plane, J. M. C.: The chemistry of meteoric metals in the $Earth's$ upper atmosphere, Int. Rev. Phys. Chem., 10, 55–106, doi:10.1080/01442359109353254, 1991.

Plane, J. M. C.: Atmospheric Chemistry of Meteoric Metals, Chem. Rev., 103, 4963–4984, doi:10.1021/cr0205309, 2003.

Plane, J. M. C.: A time-resolved model of the mesospheric Na layer: constraints on the meteor input function, Atmos. Chem. Phys., 4, 627–638, 2004.

Plane, J. M. C.: A new time-resolved model of the mesospheric Na layer: constraints on the meteor input function, Atmos. Chem. Phys. Discuss., 4, 39–69, 2004.

Raizada, S., Tepley, C. A., Janches, D., Friedman, J. S., Zhou, Q., and Mathews, J. D.: Lidar observations of Ca and K metallic layers from Arecibo and comparison with micrometeor sporadic activity, J. Atmos. Sol. Terr. Phys., 66, 595–606, doi:10.1016/j.jastp.2004.01.030, 2004.

Rapp, M. and Lübken, F.-J.: Modelling of positively charged aerosols in the polar summer mesopause region, Earth Plan. Space, 51, 799–807, 1999.

Rapp, M. and Lübken, F.-J.: Modelling of particle charging in the polar summer mesosphere: Part 1 – general results, J. Atmos. Sol. Terr. Phys., 63, 759–770, 2001.

Rapp, M. and Lübken, F.-J.: On the nature of PMSE: Electron diffusion in the vicinity of charged particles revisited, J. Geophys. Res., 108, 8437, doi:10.1029/2002JD002857, 2003.

Rapp, M. and Lübken, F.-J.: Polar mesosphere summer echoes (PMSE): Review of observations and current understanding, Atmos. Chem. Phys., 4, 2601–2633, 2004.

Rapp, M. and Strelnikova, I.: Measurements of meteor smoke particles during the ECOMA-2006 campaign: 1. particle detection by active photoionization, J. Atmos. Sol. Terr. Phys., *accepted*, 2008.

Rapp, M. and Thomas, G. E.: Modeling the microphysics of mesospheric ice particles: Assessment of current capabilities and basic sensitivities, J. Atmos. Sol. Terr. Phys., 68, 715–744, 2006.

Rapp, M., Gumbel, J., Lübken, F.-J., and Latteck, R.: D region electron number density limits for the existence of polar mesosphere summer echoes, J. Geophys. Res., 107, 4187, doi:10.1029/2001JD001323, 2002a.

Rapp, M., Lübken, F.-J., Müllemann, A., Thomas, G., and Jensen, E.: Small scale temperature variations in the vicinity of NLC: experimental and model results, J. Geophys. Res., 107, 4392, doi:10.1029/2001JD001241, 2002b.

Rapp, M., Hedin, J., Strelnikova, I., Friedrich, M., Gumbel, J., and Lübken, F.-J.: Observations of positively charged nanoparticles in the nighttime polar mesosphere, Geophys. Res. Lett., 32, L23821, doi:10.1029/2005GL024676, 2005.

Rapp, M., Strelnikova, I., and Gumbel, J.: Meteoric smoke particles: Evidence from rocket and radar techniques, Adv. Space Res., 40, 809–817, doi:10.1016/j.asr.2006.11.021, 2007.

Rapp, M., Strelnikova, I., Latteck, R., Hoffmann, P., Hoppe, U., Häggström, I., and Rietveld, M.: Polar mesosphere summer echoes (PMSE) studied at Bragg wavelengths of 2.8 m, 67 cm, and 16 cm, J. Atmos. Sol. Terr. Phys., 70, 947–961, doi:10.1016/j.jastp.2007.11.005, 2008a.

Rapp, M., Strelnikova, I., Strelnikov, B., Latteck, R., Baumgarten, G., Li, Q., Megner, L., Gumbel, J., Friedrich, M., Hoppe, U.-P., and Robertson, S.: First in situ measurement of the vertical distribution of ice volume in a mesospheric ice cloud during the ECOMA/MASS rocket-campaign, Ann. Geophys., subm., 2008b.

Rauser, P. and Fechtig, H.: Combined dust collection and detection experiment during a noctilucent cloud display above Kiruna, Sweden., in: Space Research XII, Vol. 1, p. 391 - 402, vol. 1 of *Space Research*, pp. 391–402, 1972.

Rietveld, M. T. and Collis, P. N.: Mesospheric observations with the EISCAT UHF radar during polar cap absorption events: 2. Spectral measurements, Ann. Geophys., 11, 797–808, 1993.

Robertson, S., Smiley, B., Horányi, M., Sternovsky, Z., Gumbel, J., and Stegman, J.: Rocket-Borne Probes for Charged Ionospheric Aerosol Particles, IEEE Transactions on Plasma Science, 32, 716–723, doi:10.1109/TPS.2004.826113, 2004.

Romejko, V. A., Dalin, P. A., and Pertsev, N. N.: Forty years of noctilucent cloud observations near Moscow: Database and simple statistics, J. Geophys. Res., 108, 8443–+, doi:10.1029/2002JD002364, 2003.

Rosinski, J. and Snow, R. H.: Secondary particulate matter from meteor vapors., J. Atmos. Sci., 18, 736–745, 1961.

Röttger, J. and La Hoz, C.: Characteristics of polar mesosphere summer echoes (PMSE) observed with the EISCAT 224 MHz radar and possible explanations of their origin, J. Atmos. Terr. Phys., 52, 893–906, 1990.

Röttger, J., Rietveld, M. T., La Hoz, C., Hall, T., and Kelley, M. C.: Polar mesosphere summer echoes observed with the EISCAT 933 MHz radar and the CUPRI 46.9 MHz radar, their similarity to 224 MHz radar echoes, and their relation to turbulence and electron density profiles, Radio Sci., 25, 671–687, 1990.

Rusch, D. W., Thomas, G. E., and Jensen, E. J.: Particle size distributions in polar mesospheric clouds derived from solar mesosphere explorer measurements, J. Geophys. Res., 96, 12 933–+, doi:10.1029/91JD01227, 1991.

Saunders, R. W. and Plane, J. M. C.: A laboratory study of meteor smoke analogues: Composition, optical properties and growth kinetics, J. Atmos. Solar Terr. Phys., 68, 2182–2202, doi:10.1016/j.jastp.2006.09.006, 2006.

Saunders, R. W., Forster, P. M., and Plane, J. M. C.: Potential climatic effects of meteoric smoke in the Earth's paleo-atmosphere, Geophys. Res. Lett., 34, 16 801–+, doi: 10.1029/2007GL029648, 2007.

Schulte, P. and Arnold, F.: Detection of upper atmospheric negatively charged microclusters by a rocket-borne mass spectrometer, Geophys. Res. Lett., 19, 2297–2300, 1992.

Schunk, R. W.: Transport equations for aeronomy, Planet. Space Sci., 23, 437–485, 1975.

Seele, C. and Hartogh, P.: Water vapor of the polar middle atmosphere: Annual variation and summer mesosphere conditions as observed by ground-based microwave spectroscopy, Geophys. Res. Lett., 26, 1517–1520, 1999.

Shettle, E. P., DeLand, M. T., Thomas, G. E., and Olivero, J. J.: Long term variations in the frequency of polar mesospheric clouds in the Northern Hemisphere from SBUV, Geophys. Res. Lett., 36, 2803–+, doi:10.1029/2008GL036048, 2009.

Singer, W., Bremer, J., Hocking, W. K., Weiss, J., Latteck, R., and Zechal, M.: Temperature and wind tides around the summer mesopause at middle and arctic latitudes, Adv. Space Res., 31, 2055–2060, doi:10.1016/S0273-1177(03)00228-X, 2003.

Singer, W., von Zahn, U., and Weiß, J.: Diurnal and annual variations of meteor rates at the arctic circle, Atmos. Chem. Phys., 4, 1355–1363, 2004.

Smiley, B., Robertson, S., Horanyi, M., Blix, T., Rapp, M., Latteck, R., and Gumbel, J.: Measurement of negatively and positively charged particles inside PMSE during MIDAS SOLSTICE 2001, J. Geophys. Res., 108(D8), 8444, doi: 10.1029/2002JD002425, 2003.

Strelnikova, I., Rapp, M., Raizada, S., and Sulzer, M.: Meteor smoke particle properties derived from Arecibo incoherent scatter radar observations, Geophys. Res. Lett., 34, 15 815–+, doi:10.1029/2007GL030635, 2007.

Strelnikova, I., Rapp, M., Strelnikov, B., Baumgarten, G., Brattli, A., Svenes, K., Hoppe, U.-P., Friedrich, M., Gumbel, J., and Williams, B.: Measurements of meteor smoke particles during the ECOMA-2006 campaign: 2. results, J. Atmos. Sol. Terr. Phys., ATP 2785, doi:doi:10.1016/j.jastp.2008.07.011, 2008.

Stroud, W. G., Nordberg, W., Bandeen, W. R., Bartman, F. L., and Titus, P.: Rocket-Grenade Observation of Atmospheric Heating in the Arctic, J. Geophys. Res., 64, 1342–+, doi:10.1029/JZ064i009p01342, 1959.

Summers, M. E. and Siskind, D. E.: Surface recombination of O and H_2 on meteoric dust as a source of mesospheric water vapor, Geophys. Res. Lett., 26, 1837–1840, doi: 10.1029/1999GL900430, 1999.

Tanenbaum, B. S.: Continuum theory of Thomson scattering, Phys. Rev., 171, 215–221, 1968.

Thomas, G. E.: Mesopheric clouds and the physics of the mesopause region, Rev. Geophys, 29, 553–575, 1991.

Thomas, G. E. and McKay, C. P.: On the mean particle size and water content of polar mesospheric clouds, Planet. Space Sci., 33, 1209–1224, doi:10.1016/0032-0633(85)90077-7, 1985.

Voigt, C., Schlager, H., Luo, B. P., Dörnbrack, A., Roiger, A., Stock, P., Curtius, J., Vössing, H., Borrmann, S., Davies, S., Konopka, P., Schiller, C., Shur, G., and Peter, T.: Nitric Acid Trihydrate (NAT) formation at low NAT supersaturation in Polar Stratospheric Clouds (PSCs), Atmos. Chem. Phys., 5, 1371–1380, 2005.

von Cossart, G., Fiedler, J., and von Zahn, U.: Size distributions of NLC particles as determined from 3-color observations of NLC by ground-based lidar, Geophys. Res. Lett., 26, 1513–1516, 1999.

von Savigny, C., Petelina, S. V., Karlsson, B., Llewellyn, E. J., Degenstein, D. A., Lloyd, N. D., and Burrows, J. P.: Vertical variation of NLC particle sizes retrieved from Odin/OSIRIS limb scattering observations, Geophys. Res. Lett., 32, L07806, doi: 10.1029/2004GL021982, 2005.

von Zahn, U.: Lidar observations of Meteor trails: evidence for fragmentation of meteoroids and their subsequent differential ablation, in: Proceedings of the meteorids 2001 conference, Swedish Institute of Space Physics, Kiruna, Sweden, edited by Warmbein, B., vol. ESA SP–495, pp. 303–314, 2001.

von Zahn, U.: The total mass flux of meteoroids into the Earth's upper atmosphere, in: 17th ESA Symposium on European Rocket and Balloon Programmes and Related Research, edited by Warmbein, B., vol. 590 of *ESA Special Publication*, pp. 33–39, 2005.

von Zahn, U. and Bremer, J.: Simultaneous and common-volume observations of noctilucent clouds and polar mesosphere summer echoes, Geophys. Res. Lett., 26, 1521–1524, doi: 10.1029/1999GL900206, 1999.

Vondrak, T., Plane, J. M. C., Broadley, S., and Janches, D.: A chemical model of meteoric ablation, Atmos. Chem. Phys. Discuss., 8, 14 557–14 606, 2008.

Wasson, J. T. and Kyte, F. T.: Comment on the letter 'On the influx of small comets into the earth's atmosphere. II - Interpretation', Geophys. Res. Lett., 14, 779–+, 1987.

Witt, G.: The nature of noctilucent clouds, Space Res., IX, 157–169, 1969.

Zolensky, M., Bland, P., Brown, P., and Halliday, I.: Flux of Extraterrestrial Materials, pp. 869–888, Meteorites and the Early Solar System II, 2006.

Appendix A

Tables

Table A.1: The overview of ECOMA flights in the time period from October 2004 to August 2007

	ECOMA00	ECOMA01	ECOMA02	ECOMA03
Date	28 October 2004	8 September 2006	17 September 2006	3 August 2007
Time	21:49 LT	22:17 UT	21:06 UT	23:22 UT
Latitude	$68°N$	$69°N$	$69°N$	$69°N$
Longitude	$21°E$	$16°E$	$16°E$	$16°E$
Apogee [km]	91.4	130.6	130.3	126.7
Zenith angle	120.1°	105.3°	106.5°	93.2°
Electrode surface	copper	gold	gold	gold
First grid, voltage	$-6\ V$	$+6\ V$	$+6\ V$	$-3\ V$
Second grid, voltage	$+6\ V$	$-6\ V$	$-6\ V$	$+3\ V$

Table A.2: Eiscat measurements analysed for statistics in **Paper VIII**, *Fig.* 6.

date	hours	experiment	PMSE duration
29-May-2003	15 : 00 – 16 : 00	arc-dlayerv-1.00	$\sim 1\ h$
29-May-2003	22 : 30 – 24 : 00	arc-dlayerv-1.00	$\sim 1.5\ h$
30-Jun-2003	07 : 40 – 10 : 40	arc-dlayerv-$bore - 1.10 - NO$	$\sim 3\ h$
01-Jul-2003	05 : 09 – 06 : 05	arc-dlayerv-$bore - 1.10 - NO$	$\sim 1\ h$
01-Jul-2003	08 : 20 – 12 : 15	arc-dlayerv-$bore - 1.10 - NO$	$\sim 4\ h$
02-Jul-2003	06 : 57 – 10 : 00	arc-dlayerv-$bore - 1.10 - NO$	$\sim 3\ h$
01-Aug-2003	08 : 44 – 11 : 48	arc-dlayerv-$bore - 1.10 - NO$	$\sim 3\ h$
04-Aug-2003	08 : 17 – 10 : 30	arc-dlayerv-$bore - 1.10 - NO$	$\sim 2\ h$
05-Jul-2005	07 : 00 – 13 : 00	arc-dlayerv-$htv - zenith - 1.10 - SP$	$\sim 6\ h$
14-Jun-2004	07 : 50 – 22 : 00	arc-dlayerv-$zenith - 1.11 - CP$	$\sim 13\ h$
15-Jun-2004	00 : 00 – 24 : 00	arc-dlayerv-$zenith - 1.11 - CP$	$\sim 20\ h$
28-Jun-2006	08 : 00 – 10 : 00	manda-$zenith - 1.10\text{v} - CP$	$\sim 1.5\ h$
01-Jul-2006	06 : 32 – 11 : 15	arc-dlayerv-$zenith - 1.11 - SP$	$\sim 4.5\ h$
02-Jul-2006	06 : 58 – 12 : 00	arc-dlayerv-$zenith - 1.11 - SP$	$\sim 4\ h\ 45\ m$
03-Jul-2006	09 : 28 – 12 : 00	arc-dlayerv-$zenith - 1.11 - SP$	$\sim 2.5\ h$
04-Jul-2006	08 : 30 – 12 : 45	arc-dlayerv-$zenith - 1.11 - SP$	$\sim 3\ h$
05-Jul-2006	07 : 00 – 07 : 50	arc-dlayerv-$zenith - 1.11 - SP$	$\sim 50\ m$
05-Jul-2006	09 : 00 – 14 : 00	arc-dlayerv-$zenith - 1.11 - SP$	$\sim 5\ h$
05-Jul-2006	12 : 45 – 13 : 00	manda-$zenith - 1.00u - SP$	$\sim 15\ m$
06-Jul-2006	08 : 00 – 11 : 00	arc-dlayerv-$zenith - 1.11 - SP$	$\sim 3\ h$
05-Jul-2006	12 : 20 – 13 : 40	manda-$zenith - 1.00u - SP$	$\sim 20\ m$
03-Aug-2007	22 : 10 – 23 : 50	arc-dlayerv-$zenith - 1.11 - GE$	$\sim 1.5\ h$
04-Aug-2007	22 : 10 – 00 : 00	arc-dlayerv-$zenith - 1.11 - GE$	$\sim 2\ h$
07-Aug-2007	19 : 35 – 01 : 00	arc-dlayerv-$zenith - 1.11 - GE$	$\sim 1.5\ h$
11-Aug-2007	07 : 55 – 11 : 30	arc-dlayerv-$zenith - 1.11 - GE$	$\sim 2.5\ h$
12-Aug-2007	08 : 30 – 12 : 30	arc-dlayerv-$zenith - 1.11 - GE$	$\sim 3.5\ h$

Appendix B

Definitions and abbreviations

Ablation:	Any removal of mass from a meteor body during its passage through the atmosphere.
AIM:	Aeronomy of Ice in the Mesosphere spacecraft.
ALWIN:	ALOMAR WINd radar. Operating frequency 53.5 MHz.
CARMA:	The Community Aerosol and Radiation Model for Atmospheres.
CC2D:	Combination of CARMA and CHEM2D models.
CDD:	Colorado Dust Detector.
CHEM2D:	Chemical/Dynamical Model of the Middle Atmosphere developed at Naval Research Laboratory.
Coagulation:	The creation of larger particles as a result of collisions of two or more smaller particles.
DC-current:	Current, measured by ECOMA 1 kHz channel owing to charged particles reaching the detector electrode inside the Faraday cup.
ECOMA:	Existence and Charge state Of meteor smoke particles in the Middle Atmosphere.
EISCAT:	European Incoherent SCAtter radar.
Flash-current:	Current, measured by ECOMA 100 kHz channel owing to photoelectrons emitted from particles after flash.
Head echo:	the ball of plasma around the ablating particle as it descends through the atmosphere.
HPLA:	High-Power Large Aperture radar.
IS:	Incoherent scatter. A ground-based technique for studying the earth's ionosphere. A radar beam scattering off electrons in the ionospheric plasma creates an incoherent scatter echo.
ISR:	Incoherent scatter radar.
LDEF:	Long Duration Exposure Facility satellite.
Meteoroid:	A small (sub-km) object in an independent orbit in the solar system.
Meteor:	The light phenomenon (=shooting star) produced by meteoroid experiencing strong frictional heating when entering the Earth's atmosphere.

Meteorite:	A natural object of extraterrestrial origin that has survived at least in parts its passage through the Earth's atmosphere and was collected at the Earth's surface as "stone".
Micrometeorite:	A meteorite with the size of less than about 1 mm. Large quantities of micrometeoric material from 0.1 mm to larger than 1 mm in diameter, both melted and apparently unmelted, have been recovered from e.g. the ocean floor, the Antarctic ice, and lakes in Greenland.
MLT:	Mesosphere Lover Thermosphere region.
MSPs:	Meteoric smoke particles.
NAT:	Nitric Acid Trihydrate particles.
NLC:	Noctilucent clouds are high atmosphere cloud formations composed of small ice-coated particles.
Mesosphere:	The third highest layer in our atmosphere, occupying the region 50 km to 80 km above the surface of the Earth, above the troposphere and stratosphere, and below the thermosphere.
PMC:	Polar Mesospheric Clouds (the NLC viewed from the space).
PMSE:	Polar Mesosphere Summer Echoes are very strong radar returns observed in the polar summer mesosphere.
Smoke:	Particles formed by condensation or chemical reaction from molecularly dispersed matter.
SOFIE:	The Solar Occultation For Ice Experiment was launched onboard the AIM satellite.

Appendix C

List of included publications

This thesis summarizes the following publications (stated here together with a statement about the candidate's contribution):

- **Paper I**

  M. Rapp and I. Strelnikova, Measurements of meteor smoke particles during the ECOMA-2006 campaign: 1. Particle detection by active photoionization, J. Atmos. Sol.-Terr. Phys., in press, *doi* : 10.1016/*j.jastp*.2008.06.002, 2008.

- **Paper II**

  I. Strelnikova, M. Rapp, B. Strelnikov, G. Baumgarten, A. Brattli, K. Svenes, U.-P. Hoppe, M. Friedrich, J. Gumbel, B. P. Williams. Measurements of meteor smoke particles during the ECOMA-2006 campaign: 2. Results, J. Atmos. Sol.-Terr. Phys., in press, *doi* : 10.1016/*j.jastp*.2008.07.011, 2008.

- **Paper III**

  M. Rapp, I. Strelnikova, B. Strelnikov, R. Latteck, G. Baumgarten, Q. Li, L. Megner, J. Gumbel, M. Friedrich, U.-P. Hoppe, and S. Robertson. First in situ measurement of the vertical distribution of ice volume in a mesospheric ice cloud during the ECOMA/MASS rocket-campaign. Ann. Geophys., 27, 755-766, 2009

- **Paper IV**

  M. Rapp, I. Strelnikova, and J. Gumbel. Meteoric smoke particles: Evidence from rocket and radar techniques, Adv. Space Res., 40, 809-817, doi: 10.1016/j.asr2006.11.021, 2007.

- **Paper V**

  I. Strelnikova, M. Rapp, S. Raizada, M. Sulzer. Meteor smoke particle properties derived from Arecibo incoherent scatter radar observations. Geophys. Res. Lett., 34, L15815, doi: 10.1029/2007GL030635, 2007.

- **Paper VI**

  I. Strelnikova and M. Rapp. Meteoric smoke particle signatures in D-region incoherent scatter radar spectra, Proceedings of the 18th ESA Symposium on European Rocket and Balloon Programmes and Related Research, ESA-SP-647, 629-634, 2007.

- **Paper VII**

  M. Rapp, I. Strelnikova, R. Latteck, P. Hoffmann, U.-P. Hoppe, I. Häggström, M. T. Rietveld, Polar mesosphere summer echoes (PMSE) studied at Bragg wavelengths of 2.8 m, 67 cm, and 16 cm, J. Atmos. Sol.-Terr. Phys., 70, 947-961, doi: 10.1016/j.jastp.2007.11.005, 2008.

- **Paper VIII**

  I. Strelnikova and M. Rapp. Incoherent scatter radar measurements from the D-region: What can we learn from the spectral shape?, submitted to Adv. Space Res., October 2008.

Summary

Mesospheric aerosol particles: Evidence from rocket and radar techniques

Every day, the Earth's atmosphere is hit by ~50 tons of meteoric material witch vaporizes between ~70 and 100 km. This evaporated material forms metal layers in the upper mesosphere and can recondense forming solid nanometer-scale meteor smoke particles (MSP). Under conditions of the polar summer mesopause MSP are thought to act as nuclei for ice particles which are observed as noctilucent clouds (NLC) and polar mesosphere summer echoes (PMSE).

In this work two new techniques for aerosol measurements in the mesosphere were developed and successfully applied. The first method employs a new rocket-borne instrument for in situ measurements and the second is a radar technique for ground-based remote soundings.

The rocket-borne instrument is a combination of a Faraday-Cup and a xenon-flashlamp for active photoionization of the aerosols. The measurements with this instrument delivered the first experimental confirmation for the existence of MSPs in the entire mesosphere as it was previously only predicted by models. This new instrument was also applied for measurements of ice particles and yielded the first direct in situ data of mesospheric ice volume densities at unprecedented height resolution. It also allows to measure both MSP and ice particles simultaneously.

Using powerful incoherent scatter radars it was further demonstrated that MSP can in fact be observed from the ground making use of the spectral characteristics of observed signals. Corresponding measurements constitute the first ground based detection of MSP and hence open a new observing window for the study of these particles. This new technique allows the derivation of mean radii and number densities of the aerosols particles. Application of this method to measurements with the Arecibo incoherent scatter radar in Puerto Rico yields good agreement with experimental data obtained by rocket techniques and with model results.

Finally, the current standard theory of PMSE was confirmed by two new and independent radar experiments.

Zusammenfassung

Messungen mesosphärischer Aerosolpartikel mit Höhenforschungsraketen und Radars

Die Erdatmosphäre ist täglich einem Fluss von ~50 Tonnen meteoritischen Materials ausgesetzt, welches in einem Höhenbereich von ~70-100 km verdampft. Dieses verdampfte Material bildet zum einen die bekannten Metallatomschichten und zum anderen kleine nanometergroße Meteorstaubteilchen (MSP). Von diesen wird vermutet, dass sie unter den Bedingungen der kalten polaren Sommermesopause die Nukleationskeime für Eispartikel bilden, welche als leuchtende Nachtwolken (NLC) bzw. als Polare Mesosphären Sommerechos (PMSE) beobachtet werden.

In diese Arbeit wurden zwei neuen Messmethoden entwickelt und erfolgreich angewandt. Die eine Methode basiert auf einem raketengetragenen Instrument zur direkten Messung in der Mesosphäre, während die andere Methode auf Messungen mit besonders leistungsstarken Radar-Geräten zur bodengebundenen Fernerkundung der Aerosole beruht.

Das raketengetragene Instrument kombiniert einen sogenannten Faraday-Cup mit einer Xenon-Blitzlampe, die zur Photoionisation der nachzuweisenden Partikel dient. Damit durchgeführte Messungen bestätigen erstmalig die Existenz der MSP in der gesamten Mesosphäre, was bisher nur von Modellen vorhergesagt wurde. Diese Methode wurde ferner zur Messung mesosphärischer Eispartikel eingesetzt, wobei die ersten direkten Messungen der Volumendichte solcher Partikel mit bisher unerreichter vertikaler Auflösung durchgeführt werden konnten. Ferner erlaubt diese Technik die gleichzeitige Messung von Eis- und Meteorstaubteilchen während eines Raketenfluges.

Ebenso gelang der erstmalige Nachweis von MSP in Radarmessungen, womit gezeigt wurde, dass MSP prinzipiell mit Fernerkundungsmethoden beobachtet werden können. Aus diesen Messungen wurden mittlere Radien sowie Anzahldichten der geladenen Teilchen bestimmt. Die Ergebnisse dieser Messungen mit dem Arecibo-Radar in Puerto Rico zeigen eine gute Übereinstimmung mit Modellen und anderen unabhängigen Messungen mit Raketen.

Schließlich wurde die Theorie der PMSE in dieser Arbeit mit zwei unabhängigen und neuen Radarmethoden bestätigt.

Acknowledgments

I thank my supervisor, Prof. Dr. Markus Rapp, for his invaluable help and continuous support during my life in Germany and especially my work at IAP. I am grateful to Prof. Franz-Josef Lübken for giving me this excellent opportunity to work at IAP which enabled me to produce the results of this thesis.

I greatly appreciate Prof. Martin Friedrich's contribution to all of my science projects and specifically his willingness to review this thesis.

I also greatly appreciate Prof. Jörg Gumbel's contribution to my growth as a scientists and for his help reviewing this thesis.

Hans-Jürgen Heckl has build all the hardware for our experiments and without his great work none of our rocket experiments would have been possible.

Torsten Köpnick's help and engineering support was always available whenever needed and I am grateful for that.

I would like to thank the Middle Atmosphere Group of MISU at Stockholm University: Linda Megner, Jonas Hedin, Misha Khaplanov for their collaboration and help in extending my knowledge in atmospheric science.

I thank the team from FFI: Ulf-Peter Hoppe, Stig Karsrud, Vidar Killingmo, and Terje Angeltveit for their brilliant collaboration and pleasant company during our rocket campaigns.

I specially would like to thank the scientists at Arecibo: Shika Raizada and Mike Sulzer for their excellent collaboration and support with the Arecibo-radar measurements.

I thank Esa Turunen and Antti Kero for getting me started with the EISCAT data analysis.

I thank Mike Rietveld and Jurgen Röttger for our many helpful discussions regarding the EISCAT data analysis.

I thank the company von Hörner & Sulger, especially Guido Krein for developing and supporting our ECOMA-electronics.

The DLR-Moraba (Mobile rocket base) and the staff of the Andøya Rocket Range are an inseparable part of our rocket-based research. They are highly skilled professionals and they create a friendly work environment making our collaboration very pleasant.

I thank all the IAP staff for their friendly attitude making my work at the institute very comfortable and productive. I have had many insightful conversations here at IAP contributing to the ideas in this thesis.

I would like to thank Frau Roswitha Mehl for her invaluable help in our accommodation in Kühlungsborn.

I also thank all of my friends from Kühlungsborn and Rostock for helping me integrate into German culture.

The rocket measurements were supported by the German Space Agency (DLR) under grant 50 OE 0301 (Project ECOMA).

EISCAT is an international association supported by the research councils of of Norway, Sweden, Finland, Japan, China, the United Kingdom and Germany.

The EISCAT observation were supported by the Deutsche Forschungsgemeinschaft (DFG) in the frame of the CAWSES priority program under grant RA 1400/2-1 and 1400/2-2.